

# Robust Cross-Linked Stereocomplexes and C<sub>60</sub> Inclusion Complexes of Vinyl-Functionalized Stereoregular Polymers Derived from Chemo/Stereoselective Coordination Polymerization

Fernando Vidal,<sup>†</sup> Laura Falivene,<sup>‡</sup> Lucia Caporaso,<sup>§</sup> Luigi Cavallo,<sup>\*,‡</sup> and Eugene Y.-X. Chen<sup>\*,†</sup>

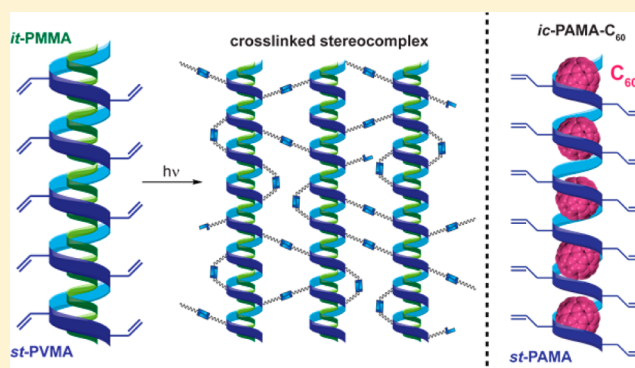
<sup>†</sup>Department of Chemistry, Colorado State University, Fort Collins, Colorado 80523-1872, United States

<sup>‡</sup>Physical Sciences and Engineering Division, Kaust Catalysis Center, King Abdullah University of Science and Technology (KAUST), Thuwal 23955-6900, Saudi Arabia

<sup>§</sup>Dipartimento di Chimica e Biologia, Università di Salerno, Via Papa Paolo Giovanni II, I-84084 Fisciano, Italy

**S** Supporting Information

**ABSTRACT:** The successful synthesis of highly syndiotactic polar vinyl polymers bearing the reactive pendant vinyl group on each repeat unit, which is enabled by perfectly chemo-selective and highly syndiospecific coordination polymerization of divinyl polar monomers developed through this work, has allowed the construction of robust cross-linked supramolecular stereocomplexes and C<sub>60</sub> inclusion complexes. The metal-mediated coordination polymerization of three representative polar divinyl monomers, including vinyl methacrylate (VMA), allyl methacrylate (AMA), and *N,N*-diallyl acrylamide (DAA) by C<sub>s</sub>-ligated zirconocenium ester enolate catalysts under ambient conditions exhibits complete chemoselectivity and high stereoselectivity, thus producing the corresponding vinyl-functionalized polymers with high (92% *rr*) to quantitative (>99% *rr*) syndiotacticity. A combined experimental (synthetic, kinetic, and mechanistic) and theoretical (DFT) investigation has yielded a unimetallic, enantiomeric-site-controlled propagation mechanism. Postfunctionalization of the obtained syndiotactic vinyl-functionalized polymers via the thiol–ene click and photocuring reactions readily produced the corresponding thiolated polymers and flexible cross-linked thin-film materials, respectively. Complexation of such syndiotactic vinyl-functionalized polymers with isotactic poly(methyl methacrylate) and fullerene C<sub>60</sub> generates supramolecular crystalline helical stereocomplexes and inclusion complexes, respectively. Cross-linking of such complexes affords robust cross-linked stereocomplexes that are solvent-resistant and also exhibit considerably enhanced thermal and mechanical properties compared with the un-cross-linked stereocomplexes.



## INTRODUCTION

Because of its unique feature that each enchaining monomer must be coordinated to the catalyst site, which can be rationally designed by tuning the electronic, steric, and symmetry properties of the ancillary ligand, metal-mediated coordination polymerization has evolved into arguably the most powerful technique for precisely controlling the polymerization stereochemistry.<sup>1</sup> In the case of vinyl monomers, a class of the technologically most important monomers, metal-mediated coordination polymerization can be categorized into coordination–insertion polymerization, typically for catalytic polymerization of nonpolar olefins as well as copolymerization of nonpolar and polar olefins,<sup>2</sup> and coordination–addition polymerization, commonly for living or quasi-living and stereospecific polymerization of conjugated polar olefins such as acrylic monomers.<sup>3,4</sup>

Specifically focusing on polar divinyl monomers, rendering their chemoselective polymerization is important for the

synthesis of vinyl-functionalized polymers, which can be postfunctionalized—through the remaining vinyl groups attached to the main chain—into a variety of useful functional materials.<sup>5</sup> However, polymerization of such monomers with complete chemoselectivity by safeguarding one of the reactive vinyl groups while selectively polymerizing the other has been a challenging task for radical polymerization (especially during the later stage),<sup>6</sup> group-transfer polymerization,<sup>7</sup> or anionic polymerization carried out at  $-20$  °C or above.<sup>8</sup> In the cases where complete chemoselectivity has been achieved utilizing Lewis pair cooperativity in Lewis pair polymerization,<sup>9</sup> the resulting un-cross-linked, soluble functional polymers exhibited a broad molecular weight distribution (*M*) and low tacticity<sup>10</sup> due to nonliving and non-stereoselective features of this polymerization. In this context, coordination–addition poly-

Received: April 20, 2016

Published: July 7, 2016

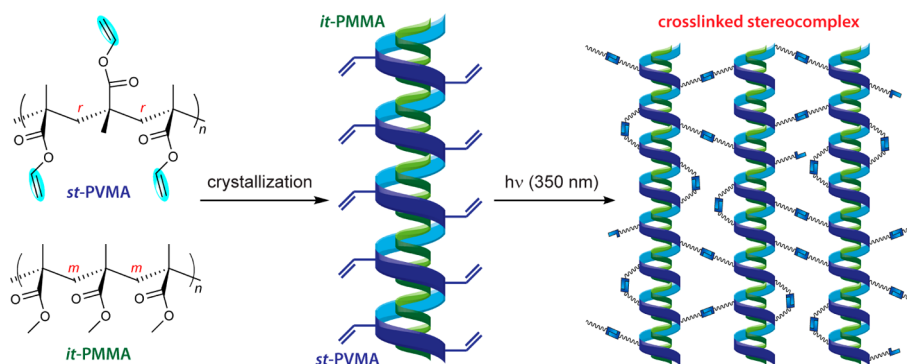


**Figure 1.** Schematic representation of the hypothesis for stereocomplexation between syndiotactic acrylic polymers carrying pendant vinyl groups and *it*-PMMA and subsequent photocuring to form robust cross-linked supramolecular structures.

merization of divinyl polar monomers is advantageous because of its high degree of control over the polymerization characteristics, even at ambient temperature. For instance, the polymerization of allyl methacrylate (AMA) by half-metallocene yttrium catalysts was shown to be both living and chemoselective.<sup>11</sup> Furthermore, a chiral  $C_2$ -ligated *ansa*-zirconocenium ester enolate complex,  $[\text{rac-C}_2\text{H}_4(\eta^5\text{-indenyl})_2\text{Zr}(\text{THF})]^+[\text{OC}(\text{O}^i\text{Pr})=\text{CMe}_2][\text{MeB}(\text{C}_6\text{F}_5)_3]^-$  (**1**),<sup>12</sup> which is known to mediate stereospecific and living polymerization of simple alkyl methacrylates such as methyl methacrylate (MMA)<sup>12,13</sup> and acrylamides,<sup>14</sup> is not only completely chemoselective and living but also highly isospecific in the polymerization of polar divinyl monomers at ambient temperature.<sup>15</sup> The origin of the perfect chemoselectivity and high isoselectivity arises from the catalyst-site-controlled coordination–addition mechanism that dictates exclusive conjugate additions across the methacrylic double bond, which is activated via coordination of the conjugated carbonyl to the cationic, chiral Zr center, thus leaving the pendant  $\text{C}=\text{C}$  bond intact.

Stereocomplexation between a pair of diastereomeric polymer chains of isotactic (*it*) and syndiotactic (*st*) poly(methyl methacrylate) (PMMA) in a typical *it*-PMMA/*st*-PMMA ratio of 1:2, when annealed in the solid state or crystallized in suitable solvents, generates a crystalline stereocomplex, *sc*-PMMA, representing a rare example of a helical supramolecular structure based on a vinyl polymer.<sup>16</sup> Polar donor solvents such as acetone, tetrahydrofuran (THF), dimethyl sulfoxide, and *N,N*-dimethylformamide (DMF) are known to promote such stereocomplexation and are thus termed complexing solvents, while chlorinated solvents such as chloroform and dichloromethane decomplex the *sc*-PMMA polymer pair and are accordingly called noncomplexing or decomplexing solvents. Although the structure of *sc*-PMMA has received several revisions since the first report of the *sc*-PMMA structure model,<sup>17</sup> its formation can be readily identified or characterized by gelation or precipitation of the crystalline complex in a complexing solvent, a high endothermic melting transition temperature ( $T_m$  up to 210 °C) as determined by differential scanning calorimetry (DSC), and a characteristic diffraction peak ( $2\theta \approx 4.35^\circ$ ) observed by powder X-ray diffraction (pXRD).<sup>18,19</sup> It is worth noting here that the formation of *sc*-PMMA was reported to be restricted to *it*-PMMA but that the ester group of the *st* counterpart can be modified to extend to other *st*-poly(methacrylate)s.<sup>19</sup> In addition, the formation of *sc*-PMMA is not limited to blending of the preformed *it*- and *st*-PMMA diastereomeric polymer pair,

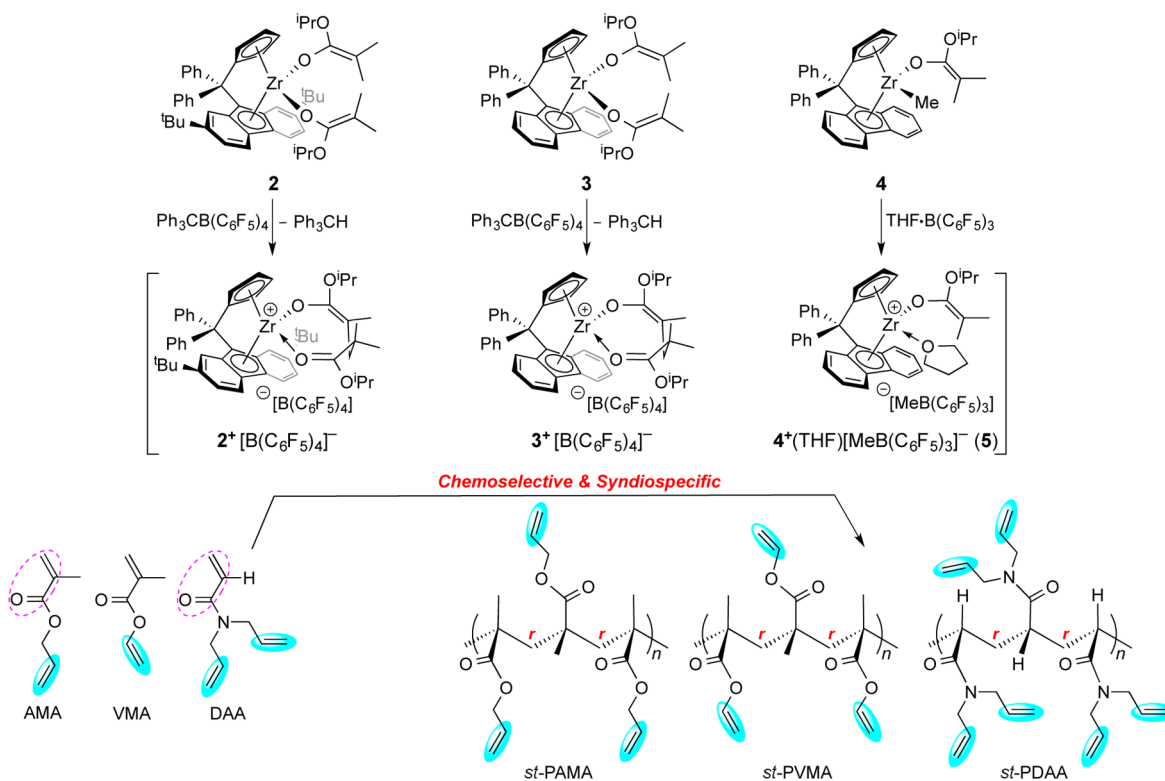
as in situ stereocomplexing polymerization of MMA using a pair of diastereospecific coordination polymerization catalysts has led to rapid, high-yield, ambient-temperature production of *sc*-PMMA with a high  $T_m$  of up to 217 °C.<sup>20</sup> Furthermore, supramolecular *sc*-PMMA/silicate nanocomposites<sup>21</sup> were fabricated by mixing dilute THF solutions of in situ-polymerized *it*-/*st*-PMMA/silicates,<sup>22</sup> and crystalline hybrid polymer stereocomplexes between polyhedral oligomeric silsesquioxane (POSS) and end-capped *it*- and *st*-PMMA–POSS chains were also synthesized.<sup>23</sup> Lastly, because of its large helical cavity ( $\sim 1$  nm), syndiotactic *st*-PMMA, which does not crystallize by itself, cocrystallizes with specific organic solvents such as benzene<sup>24</sup> and encapsulates guest nanocages such as fullerenes  $\text{C}_{60}$  and  $\text{C}_{70}$ <sup>25</sup> and MA-POSS<sup>23</sup> to form unique crystalline helical inclusion complexes.

In light of the above-overviewed unique ability of highly syndiotactic *st*-PMMA to form helical supramolecular structures of stereo- and inclusion complexes, we hypothesized that highly syndiotactic vinyl-functionalized poly(methacrylate)s, synthesizable from the proposed chemoselective and syndiospecific coordination polymerization of divinyl monomers, should form stereocomplexes with *it*-PMMA and inclusion complexes with  $\text{C}_{60}$  that, after cross-linking, should lead to robust solvent- and thermally resistant cross-linked stereocomplexes (Figure 1) and inclusion complexes. Such robust supramolecular stereocomplexes should solve the problem of decomplexation of the current stereocomplex and inclusion complex structures in noncomplexing solvents and also enhance the thermal and mechanical properties of the material. Accordingly, this report presents a full account of our work toward this central objective, which involves first achieving chemoselective and syndiospecific polymerization of divinyl polar monomers to synthesize highly syndiotactic vinyl-functionalized polymers, next postfunctionalizing and photo-cross-linking such polymers into functional materials, and finally complexing such polymers to form robust supramolecular stereo- and inclusion complexes followed by cross-linking.

## RESULTS AND DISCUSSION

**Chemoselective and Syndiospecific Polymerization of Polar Divinyl Monomers.** The first task of this study was to synthesize highly syndiotactic acrylic polymers carrying pendant vinyl groups via the development of chemoselective and syndiospecific polymerization. Previous reports from our group have shown that neutral  $C_5$ -ligated zirconocenium ester enolate complexes (pre-catalysts) such as  $[\text{Ph}_2\text{C}(\text{Cp})(2,7\text{-}^t\text{Bu}_2\text{-Flu})]\text{Zr}[\text{OC}(\text{O}^i\text{Pr})=\text{CMe}_2]_2$  (**2**) ( $\text{Cp} = \eta^5\text{-cyclopentadienyl}$ ;

Scheme 1. Chemoselective and Syndiospecific Polymerization of Polar Divinyl Monomers and Structures of Monomers, Catalysts, and Polymers Involved in This Study

Table 1. Polymerizations of Polar Divinyl Monomers (M) by Precatalysts 2–4<sup>a</sup>

run	M	precat.	activator	temp (°C)	time (min)	conv. <sup>b</sup> (%)	M <sub>n</sub> <sup>c</sup> (kg/mol)	D <sup>c</sup>	[rr] <sup>d</sup> (%)	[mr] <sup>d</sup> (%)	[mm] <sup>d</sup> (%)
1	AMA	2	[Ph <sub>3</sub> C][B]	25	180	92.7	55.3	1.33	87.9	10.6	1.5
2	AMA	3	[Ph <sub>3</sub> C][B]	25	60	55.1	35.0	1.56	92.4	6.0	1.6
3	AMA	4	[B]	25	60	53.0	24.5	1.32	90.7	7.4	1.9
4	VMA	2	[Ph <sub>3</sub> C][B]	25	60	96.2	42.9	1.40	87.0	10.5	2.5
5	VMA	3	[Ph <sub>3</sub> C][B]	25	30	98.3	42.5	1.38	92.4	7.0	0.6
6	VMA	4	[B]	25	30	98.5	41.2	1.36	93.0	6.4	0.6
7	VMA	4	[B]·THF	25	10	100	42.5	1.36	93.5	6.1	0.4
8	VMA	3	[Ph <sub>3</sub> C][B]	0	30	100	86.7	1.21	95.7	2.9	1.4
9	VMA	4	[B]·THF	0	30	97.0	98.3	1.17	94.8	3.5	1.7
10	DAA	3	[Ph <sub>3</sub> C][B]	25	10	89.0	47.5	1.34	>99	–	–
11	DAA	4	[B]·THF	25	10	94.5	42.9	1.29	>99	–	–

<sup>a</sup>Conditions: activator ([Ph<sub>3</sub>C][B] = [Ph<sub>3</sub>C][B(C<sub>6</sub>F<sub>5</sub>)<sub>4</sub>], [B] = B(C<sub>6</sub>F<sub>5</sub>)<sub>3</sub>); solvent (3.0 mL) (CH<sub>2</sub>Cl<sub>2</sub> for runs 1–9, toluene for runs 10 and 11); [M]/[cat] = 200; preactivation method (premixing of precatalyst with activator followed by addition of monomer), except for runs 3 and 6, where the *in-reactor* activation method (premixing of monomer with activator followed by addition of precatalyst) was used. <sup>b</sup>Monomer (M) conversions measured by <sup>1</sup>H NMR spectroscopy. <sup>c</sup>Number-average molecular weights (M<sub>n</sub>) and dispersities (D = M<sub>w</sub>/M<sub>n</sub>) determined by gel-permeation chromatography relative to PMMA standards. <sup>d</sup>Tacticities measured by <sup>1</sup>H or <sup>13</sup>C NMR spectroscopy in CDCl<sub>3</sub>.

Flu = η<sup>n</sup>-fluorenyl, [Ph<sub>2</sub>C(Cp)(Flu)]Zr[OC(O<sup>i</sup>Pr)=CMe<sub>2</sub>]<sub>2</sub> (3), and [Ph<sub>2</sub>C(Cp)(Flu)]ZrMe[OC(O<sup>i</sup>Pr)=CMe<sub>2</sub>] (4) can be readily activated either with [Ph<sub>3</sub>C][B(C<sub>6</sub>F<sub>5</sub>)<sub>4</sub>] (via hydride abstraction followed by Michael addition) or with B(C<sub>6</sub>F<sub>5</sub>)<sub>3</sub> or THF·B(C<sub>6</sub>F<sub>5</sub>)<sub>3</sub> (via methide abstraction) to generate the corresponding cationic complexes (catalysts) 2<sup>+</sup>[B(C<sub>6</sub>F<sub>5</sub>)<sub>4</sub>]<sup>-</sup>, 3<sup>+</sup>[B(C<sub>6</sub>F<sub>5</sub>)<sub>4</sub>]<sup>-</sup>, 4<sup>+</sup>[MeB(C<sub>6</sub>F<sub>5</sub>)<sub>3</sub>]<sup>-</sup>, and 4<sup>+</sup>(THF)[MeB(C<sub>6</sub>F<sub>5</sub>)<sub>3</sub>]<sup>-</sup> (5) (Scheme 1).<sup>26</sup> Such cationic complexes have been shown to promote rapid and syndiospecific polymerization of MMA at ambient temperature to produce highly syndiotactic *st*-PMMA with syndiotacticity up to 94% *rr*, proceeding through a monometallic, catalyst-site-controlled coordination–addition polymerization mechanism via eight-

membered-ring ester enolate intermediates.<sup>26</sup> Accordingly, 2<sup>+</sup>[B(C<sub>6</sub>F<sub>5</sub>)<sub>4</sub>]<sup>-</sup>, 3<sup>+</sup>[B(C<sub>6</sub>F<sub>5</sub>)<sub>4</sub>]<sup>-</sup>, 4<sup>+</sup>[MeB(C<sub>6</sub>F<sub>5</sub>)<sub>3</sub>]<sup>-</sup> (generated by *in-reactor* activation), and 5 (generated by preactivation) were employed for the current investigation into the polymerization of the three representative polar divinyl monomers, AMA, vinyl methacrylate (VMA), and *N,N*-diallyl acrylamide (DAA), aiming to achieve chemoselective and syndiospecific polymerization of such monomers and thus produce the corresponding highly syndiotactic polar vinyl polymers carrying a pendant C=C bond in every repeat unit (Scheme 1).

Selected results for the polymerizations of the three representative polar divinyl monomers by precatalysts 2–4 are summarized in Table 1. At the outset, control runs showed

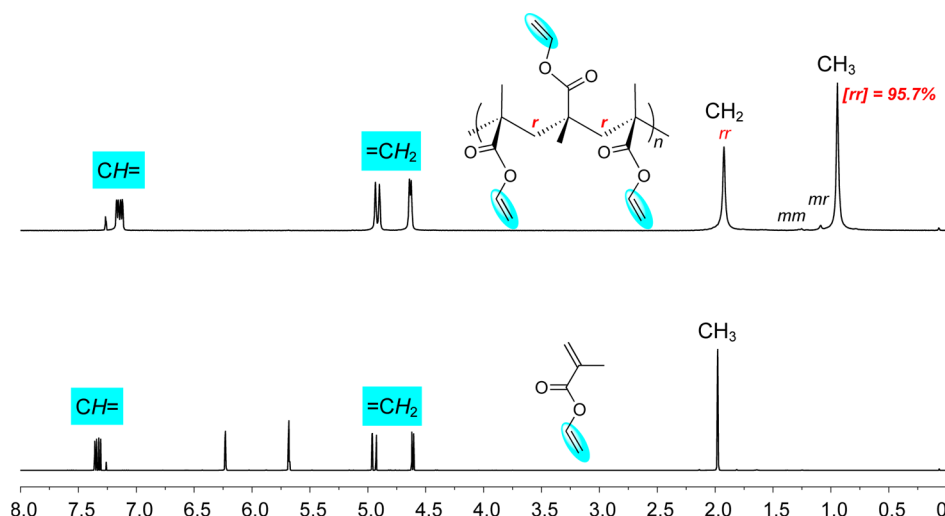


Figure 2. Overlay of the  $^1\text{H}$  NMR spectra ( $\text{CDCl}_3$ , 25  $^\circ\text{C}$ ) of VMA and *st*-PVMA.

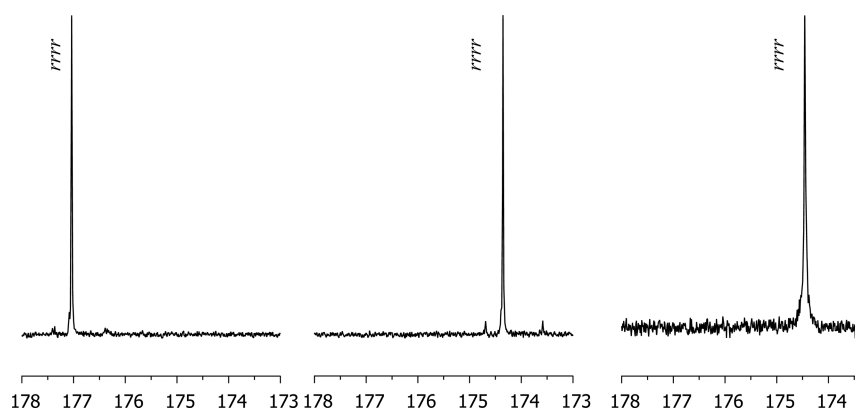


Figure 3.  $^{13}\text{C}$  NMR spectra ( $\text{CDCl}_3$ , 50  $^\circ\text{C}$ ) showing the C=O pentad (*rrrr*) region for *st*-AMA (left, run 2), *st*-PVMA (center, run 8), and *st*-PDAA (right, run 10).

that neither the neutral precatalyst nor the activator itself exhibited any activity toward such monomers. In contrast, the cationic complexes  $2^+[\text{B}(\text{C}_6\text{F}_5)_4]^-$ ,  $3^+[\text{B}(\text{C}_6\text{F}_5)_4]^-$ , and  $4^+[\text{MeB}(\text{C}_6\text{F}_5)_3]^-$ , derived from activation with  $[\text{Ph}_3\text{C}][\text{B}(\text{C}_6\text{F}_5)_4]$  (for bisenolate precatalysts 2 and 3) or  $\text{B}(\text{C}_6\text{F}_5)_3$  (for mono-enolate precatalyst 4), are highly active, quantitatively chemoselective, and also syndiospecific for polymerizations of such polar divinyl monomers at ambient temperature. Starting with the AMA polymerization in  $\text{CH}_2\text{Cl}_2$  at 25  $^\circ\text{C}$ ,  $3^+[\text{B}(\text{C}_6\text{F}_5)_4]^-$  (0.5 mol % loading) afforded *st*-PAMA with a high syndiotacticity of  $[\text{rr}] = 92.4\%$  and perfect chemoselectivity (Figure S2) but achieved a maximum monomer conversion of only 55% in 1 h (run 2). The cationic complex  $4^+[\text{MeB}(\text{C}_6\text{F}_5)_3]^-$  performed similarly (run 3 vs 2). Interestingly,  $2^+[\text{B}(\text{C}_6\text{F}_5)_4]^-$ , the more electron-rich and sterically encumbered catalyst with two *tert*-butyl substituents on the Flu ring, achieved a much higher monomer conversion of 92.7% and thus a higher-molecular-weight polymer ( $M_n = 55.3$  kg/mol,  $\mathcal{D} = 1.33$ ), but it produced *st*-PAMA with a lower syndiotacticity of  $[\text{rr}] = 87.9\%$  (run 1). The isolated *st*-PAMA ( $M_n = 35.0$  kg/mol,  $[\text{rr}] = 92\%$ ; run 2) is soluble in common organic solvents and exhibited a glass transition temperature ( $T_g$ ) of 54  $^\circ\text{C}$  as measured by DSC, which is considerably higher than that of the counterpart *it*-PAMA ( $-13$  to 0  $^\circ\text{C}$ , in the order of increasing  $M_n$ ).<sup>15</sup> A thermal cross-linking exothermic peak with an onset

temperature of 142  $^\circ\text{C}$  and a peak maximum of  $>200$   $^\circ\text{C}$  was also observed on the DSC curve.

Moving to VMA polymerization, all three  $\text{C}_s$ -ligated catalysts are perfectly chemoselective and highly syndiospecific. Again, the two catalysts without the *tert*-butyl substitution,  $3^+[\text{B}(\text{C}_6\text{F}_5)_4]^-$  and  $4^+[\text{MeB}(\text{C}_6\text{F}_5)_3]^-$ , exhibited similar polymerization characteristics (run 5 vs 6), including high activity ( $>98\%$  conversion in 30 min), medium molecular weight ( $M_n = 41.2$ – $42.5$  kg/mol), medium dispersity ( $\mathcal{D} = 1.36$ – $1.38$ ), and high syndiotacticity ( $[\text{rr}] = 92.4\%$  and  $93.0\%$ ). The polymerization by cation 5  $\{=4(\text{THF})^+[\text{MeB}(\text{C}_6\text{F}_5)_3]^-$ , generated from the reaction of 4 and  $\text{THF}\cdot\text{B}(\text{C}_6\text{F}_5)_3$ ; Scheme 1} was even more rapid, achieving 100% monomer conversion in only 10 min without signs of gel formation and also producing *st*-PVMA with a high syndiotacticity of  $[\text{rr}] = 93.5\%$  (run 7). When the polymerizations were carried out at 0  $^\circ\text{C}$ , quantitative or near-quantitative conversion was still achieved, but the molecular weights of the resulting polymers were much higher and the dispersities became narrower:  $M_n = 86.7$  kg/mol,  $\mathcal{D} = 1.21$ ,  $[\text{rr}] = 95.7\%$  by  $3^+[\text{B}(\text{C}_6\text{F}_5)_4]^-$  (run 8);  $M_n = 98.3$  kg/mol,  $\mathcal{D} = 1.17$ ,  $[\text{rr}] = 94.8\%$  by 5 (run 9). The chemoselectivity of the VMA polymerization was also perfect, as revealed by the complete disappearance of the methacrylic  $=\text{CH}_2$  proton signals at 6.23 and 5.68 ppm and the complete retention of the pendant vinyl group  $-\text{CH}=\text{CH}_2$  proton signals centered at 7.14, 4.91, and 4.63 ppm (Figure 2),

indicating that the polymerization proceeded exclusively through conjugate addition across the methacrylic double bond. Significantly, analysis of the triad stereoregularity of the resulting *st*-PVMA gave  $2[mm]/[mr] \approx 1$  (0.97 for both runs 8 and 9), indicative of an enantiomorphic-site-controlled mechanism. Furthermore, the  $^{13}\text{C}$  NMR spectrum of the polymer in the C=O pentad (*rrrr*) region provided corroborative evidence of the formation of highly syndiotactic *st*-PVMA (Figure 3). DSC analysis of the highly syndiotactic *st*-PVMA showed a  $T_g$  of  $\sim 100$  °C, which is considerably higher than that of *at*-PVMA (44–49 °C),<sup>15</sup> as well as a thermal cross-linking exothermic peak with an onset temperature of 153 °C and a peak maximum of 184 °C. We also examined the degree of polymerization control over the molecular weight by varying the  $[\text{VMA}]/[\text{S}]$  ratio from 100 to 900 (0.11 mol % catalyst loading) in  $\text{CH}_2\text{Cl}_2$  at ambient temperature, all of which runs proceeded to high conversions without signs of gel formation. The  $M_n$  value of the resulting *st*-PVMA increased linearly ( $R^2 = 0.992$ ) from 29.6 kg/mol ( $\bar{D} = 1.28$ ) to 164 kg/mol ( $\bar{D} = 1.48$ ) as the  $[\text{VMA}]/[\text{S}]$  ratio was increased from 100 to 900 (Figure 4), showing the ability of this polymerization system to control the resulting polymer molecular weight while maintaining a relatively low dispersity.

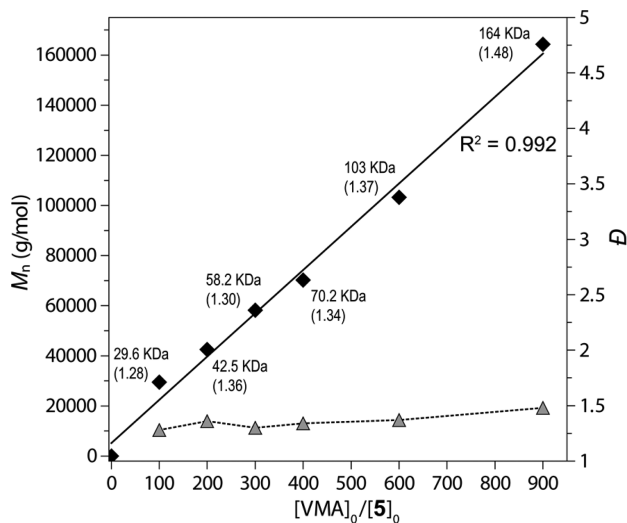


**Figure 4.** Plots of  $M_n$  (kg/mol or kDa) and  $\bar{D}$  (shown in parentheses) of *st*-PVMA produced by **5** vs the  $[\text{VMA}]_0/[\text{S}]_0$  ratio ( $\text{CH}_2\text{Cl}_2$ , 23 °C).

The chemoselectivity and stereospecificity of  $3^+[\text{B}(\text{C}_6\text{F}_5)_4]^-$  and **5** toward the polymerization of DAA were also carefully examined. Remarkably, these polymerizations not only were rapid, achieving conversions of 89.0% (run 10) and 94.5% (run 11) in 10 min, but also exhibited both quantitative chemoselectivity (Figure S3) and syndiospecificity ( $[rr] > 99\%$ ; Figure 3). DSC analysis of the highly syndiotactic *st*-PDAA showed a  $T_g$  of 35.8 °C as well as a thermal cross-linking exothermic peak with an onset temperature of 216 °C and a peak maximum of 290 °C. It is also worth noting that *st*-PDAA is soluble in common solvents of a wide polarity range, including MeOH, DMF, THF, acetone,  $\text{CHCl}_3$ ,  $\text{Et}_2\text{O}$ , and toluene, whereas *it*-PDAA was found to be soluble only in a limited number of solvents such as  $\text{CHCl}_3$  and  $\text{CH}_2\text{Cl}_2$ . In comparison, the initiator efficiency ( $I^*$ ), calculated as  $I^* = M_n(\text{calcd})/M_n(\text{exptl})$ , where  $M_n(\text{calcd}) = (\text{monomer MW}) \times [\text{M}]_0/$

$[\text{Zr}]_0 \times (\% \text{ conversion}) + (\text{MW of chain-end groups})$ , was in the range of 43–55% for AMA polymerization at room temperature, 51–54% for VMA polymerization at room temperature, and 57–67% for DAA polymerization at room temperature.

**Mechanism of Polymerization.** Next, we examined the kinetics of VMA polymerization by catalyst **5** and found that the polymerization is first order with respect to monomer concentration  $[\text{VMA}]$  for all six  $[\text{VMA}]_0/[\text{S}]_0$  ratios investigated (150 to 500) (Figure 5). A double logarithm plot of the

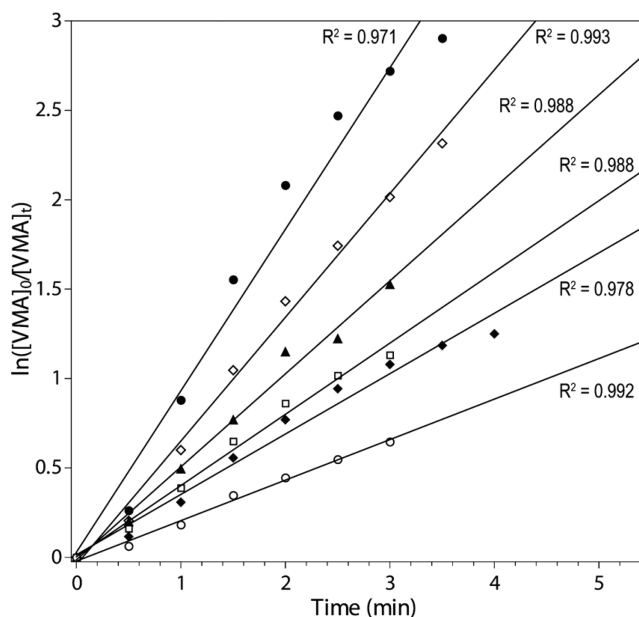


**Figure 5.** Plots of  $\ln\{[\text{VMA}]_0/[\text{VMA}]_t\}$  vs time for the polymerization of VMA by **5** in  $\text{CH}_2\text{Cl}_2$  at 23 °C. Conditions:  $[\text{VMA}]_0 = 0.832$  M;  $[\text{S}]_0 = 5.55$  mM (●), 4.16 mM (◇), 3.33 mM (▲), 2.77 mM (□), 2.07 mM (◆), 1.66 mM (○).

apparent rate constants ( $k_{\text{app}}$ ), obtained from the slopes of the best-fit lines for the plots of  $\ln\{[\text{VMA}]_0/[\text{VMA}]_t\}$  vs time, as a function of  $\ln([\text{S}]_0)$  was fit to a straight line ( $R^2 = 0.986$ ) with a slope of 1.1 (Figure 6). Thus, the kinetic order with respect to  $[\text{S}]$ , given by the slope of  $\sim 1$ , reveals that the propagation is also first order with respect to the catalyst concentration. These results indicate that the resting state in the proposed monometallic propagation “catalytic” cycle (Scheme 2) is the cyclic ester enolate **B**, which was structurally modeled by the isolated cationic cyclic ester enolate complex **6** (vide infra), and that associative displacement of the coordinated ester group by incoming monomer to regenerate the active species **A** (structurally modeled by complex **5**) is the rate-determining step (i.e., **B**  $\rightarrow$  **A**, Scheme 2). These key features of the mechanism are the same as those already established for the coordination–addition polymerization of alkyl methacrylates.<sup>3b,13,26</sup>

To provide further evidence to support the mechanism outlined in Scheme 2, cation **5** was reacted with 1 equiv of VMA to cleanly generate the corresponding single-monomer-addition product, the eight-membered metallacycle<sup>27</sup> resting intermediate  $\{[\text{Ph}_2\text{C}(\text{Cp})(\text{Flu})\text{Zr}[\text{OC}(\text{OCH}=\text{CH}_2)=\text{CMe}-\text{CH}_2\text{C}(\text{Me}_2)\text{C}(\text{O}^-\text{Pr})=\text{O}]]^+[\text{MeB}(\text{C}_6\text{F}_5)_3]^-$  (**6**) (Figure 7). This intermediate can also be generated and isolated in >91% yield via the 1:1 ratio reaction of the precatalyst **4** with the borane–monomer adduct  $\text{VMA}\cdot\text{B}(\text{C}_6\text{F}_5)_3$  (see the Supporting

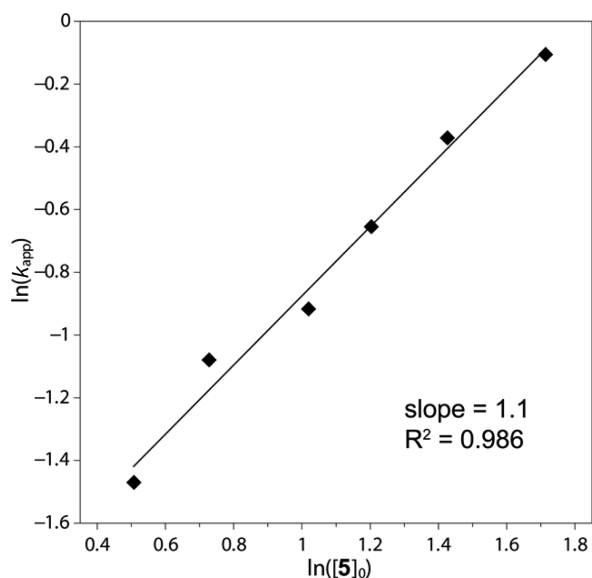
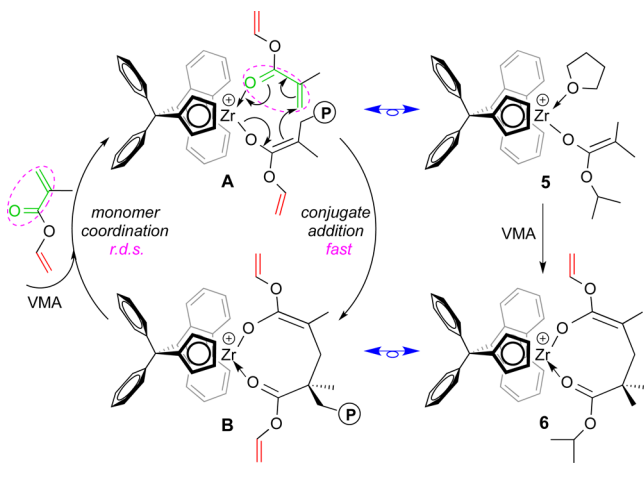


**Figure 6.** Plot of  $\ln(k_{app})$  vs  $\ln([S]_0)$  for the polymerization of VMA by **5** in  $\text{CH}_2\text{Cl}_2$  at  $23^\circ\text{C}$ .

**Scheme 2. Proposed Mechanism (Propagation “Catalytic” Cycle) for the Chemoselective and Syndiospecific Polymerization of VMA and the Structures of **5** and **6** as Synthetic Structural Models for the Active Species **A** and Resting-State Chelate **B**, Respectively**



Information (SI) for procedures and characterizations). Likewise, the metallacycle corresponding to the first AMA addition intermediate  $\{[\text{Ph}_2\text{C}(\text{Cp})(\text{Flu})\text{Zr}[\text{OC}(\text{OCH}_2\text{CH}=\text{CH}_2)=\text{CMeCH}_2\text{C}(\text{Me}_2)\text{C}(\text{O}^i\text{Pr})=\text{O}]]^+[\text{MeB}(\text{C}_6\text{F}_5)_3]^-$  (**7**) was generated in a similar fashion (see the SI and Figure S4). The successful generation and isolation of the first-monomer-addition product **6**, serving as a structural model of the resting intermediate **B**, implies that the monomer addition is fast relative to the monomer coordination in the propagation “catalytic” cycle depicted in Scheme 2 (otherwise, only polymers or oligomers plus unreacted **5** or **4** would be formed). Importantly, addition of excess VMA to a solution of **6** brought about rapid polymerization of VMA into *st*-PVMA, thereby confirming cation **6** as the resting intermediate of the catalytic cycle by this kinetic competence check. Overall, all of the experimental evidence to date is consistent with the polymerization mechanism depicted in Scheme 2.

**Mechanism of Stereoselection.** Next, we investigated the mechanism of stereoselection by a density functional theory (DFT) computational study. This needed study was prompted by the interesting observation that while the polymerizations of AMA and VMA by the  $\text{C}_2$ -ligated catalyst **1** were drastically different, leading to the formation of highly isotactic PAMA with  $[mm] = 95\text{--}97\%$  and isotactic-biased PVMA with  $[mm] = 51\text{--}53\%$ , respectively,<sup>15</sup> the polymerizations of both AMA and VMA by the  $\text{C}_s$ -ligated catalysts afforded highly syndiotactic polymers, with an even higher syndiotacticity of  $[rr] = 94\text{--}96\%$  achieved for the VMA polymerization (vide supra). Thus, it is intriguing that the placement of the  $\text{sp}^3$ -hybridized  $\text{CH}_2$  group between the ester oxygen atom and the  $\text{sp}^2$ -hybridized vinyl moiety in the case of AMA substantially enhanced the isospecificity of the polymerization but had no effect on (or even slightly reduced) the syndiospecificity of the polymerization relative to VMA without the  $\text{CH}_2$  group. This highlights the importance of the sterics and orientation of the ester OR group of the methacrylate monomer in the transition state (TS) structure that determines the stereospecificity of the metallocene-catalyzed polymerization.<sup>26a,28</sup> Accordingly, DFT calculations were performed to rationalize the high isospecificity in AMA polymerization and the low isospecificity in VMA polymerization by  $\text{C}_2$ -ligated catalyst **1** (the EBI-Zr) system as well as the high syndiospecificity in the polymerizations of both AMA and VMA with  $\text{C}_s$ -ligated catalyst **5** [the  $\text{Ph}_2\text{C}(\text{Cp})(\text{Flu})\text{Zr}$ ] system.

We calculated all of the TSs for AMA and VMA additions involving the *re* and *si* prochiral faces of the growing chain by considering geometries in which the pendant group of the monomer and that of the chain are located on opposite sides (trans) or on the same side (cis) of the metallocene equatorial belt. In addition, for the  $\text{C}_2$ -symmetric EBI-Zr system, the  $g^+$  and  $g^-$  conformations of the metallocene bridge were considered.<sup>28</sup> In all of the geometries, a *t*-Bu group was used to model the remainder of the growing chain. For the sake of simplicity, we anticipated that with the (*S,S*)-EBI-Zr-based system all of the competitive geometries show a  $g^+$  conformation of the metallocene bridge. The favored TS involves the *si* face of the chain and shows a trans geometry, whereas the cis geometry is favored for the competitive *re*-face addition with both monomers. Finally, with the (*S*)- $\text{Ph}_2\text{C}(\text{Cp})(\text{Flu})\text{Zr}$  system, a trans geometry is favored in both TSs.<sup>26a,28</sup>

The geometries and corresponding relative free energies  $\Delta G_{\text{Stereo}}$  (in kcal/mol, in dichloromethane) of the competitive TSs are reported in Figure 8 for **1** and Figure 9 for **5** with both monomers. Focusing on AMA addition, with **1** the TS involving the *si* face of the growing chain is favored by a  $\Delta G_{\text{Stereo}}$  of 5.6 kcal/mol (Figure 8, a vs b). Competition is with addition on the *re* face, which is disfavored by steric repulsion between the six-membered ring of the indenyl ligand and the  $-\text{OR}$  group of the growing chain. To alleviate this steric clash, the pendant  $-\text{OR}$  group of the chain rotates away from the indenyl ligand, resulting in a gauche conformation of the  $\text{C}1\text{--C}2\text{--O}3\text{--C}4$  dihedral angle (Figure 8b). In contrast, in the favored *si*-face addition TS, the  $\text{C}1\text{--C}2\text{--O}3\text{--C}4$  dihedral angle is much closer to the ideal trans value (Figure 8a). The high  $\Delta G_{\text{Stereo}}$  of 5.6 kcal/mol is in qualitative agreement with the high isotacticity of the obtained PAMA.

The competitive TSs geometries associated with VMA addition are compared in Figure 8c,d. In this case, addition on the *si* face is favored by a  $\Delta G_{\text{Stereo}}$  of 3.1 kcal/mol over

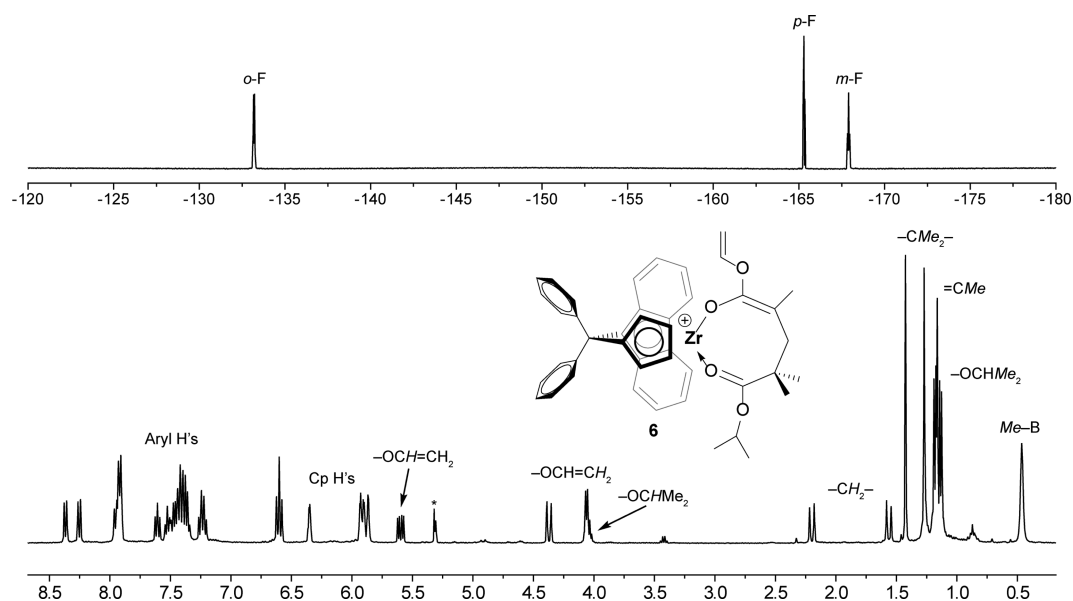


**Figure 7.** (top)  $^{19}\text{F}$  and (bottom)  $^1\text{H}$  NMR spectra ( $\text{CD}_2\text{Cl}_2$ , 25 °C, residual NMR peaks labeled as \*) of the isolated cationic complex **6**. The anion  $[\text{MeB}(\text{C}_6\text{F}_5)_3]^-$  has been omitted for clarity.

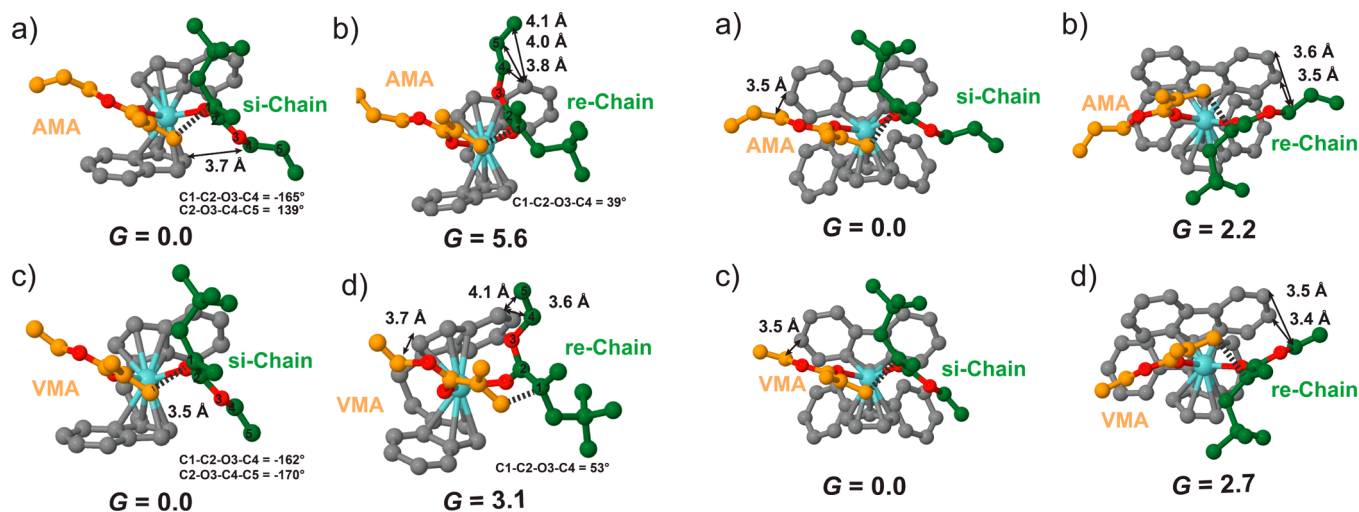


**Figure 8.** Transition state geometries for the competitive addition at the (a, c) *si* and (b, d) *re* faces of the growing chain for (a, b) AMA and (c, d) VMA with the (*S,S*)-EBI-Zr system (**1**). The free energies (in kcal/mol, in DCM) are relative to the TS involving the *si* face of the growing chain (a, c). The dashed lines indicate the emerging C–C bonds.

addition on the *re* face. As for AMA, the TS for addition on the *re* face is disfavored by the steric interaction between the pendant group of the chain and the indenyl ligand, resulting in a less stable conformation assumed by the growing chain, with a C1–C2–O3–C4 dihedral angle of 53° (Figure 8d). Although still rather large in absolute value, the  $\Delta G_{\text{Stereo}}$  of 3.1 kcal/mol calculated for VMA is 2.5 kcal/mol lower than that calculated for AMA, in qualitative agreement with the observed much lower isotacticity of the produced PVMA. The reduced stability of the favored *si*-face TS for VMA is responsible for the observed lower selectivity in the polymerization of VMA relative to AMA: the different nature of the ester carbon in the chain ( $\text{sp}^2$  for VMA vs  $\text{sp}^3$  for AMA) induces a different steric interaction between the chain and the metallocene skeleton, mainly in the favored *si*-face TSs (Figure 8, a vs c). In fact,

**Figure 9.** Transition state geometries of the competitive addition at the (a, c) *si* and (b, d) *re* faces of the growing chain for (a, b) AMA and (c, d) VMA with the (*S*)- $\text{Ph}_2\text{C}(\text{Cp})\text{Flu-Zr}$  system (**5**). The free energies (in kcal/mol, in DCM) are relative to the TS involving the *si* face of the growing chain (a, c). The dashed lines indicate the emerging C–C bonds.

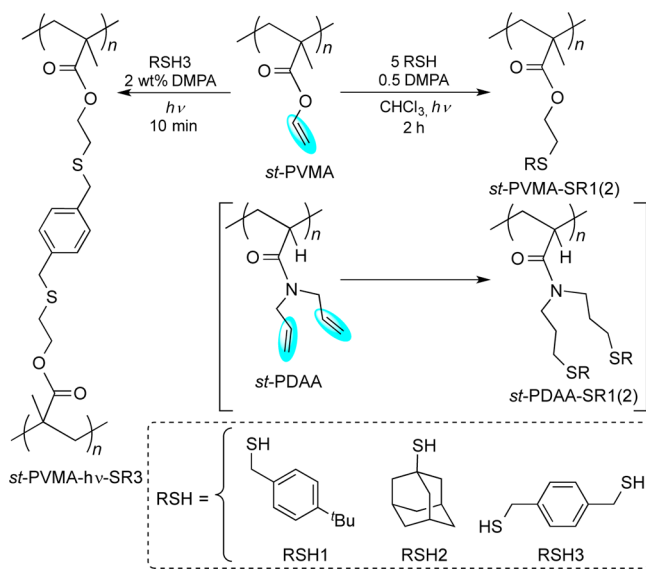
despite the fact that the *si* chain is located in the open part of the catalyst, away from the six-membered ring of the indenyl ligand, in the case of VMA the rigid  $-\text{O}-\text{CH}=\text{CH}_2$  group is forced to be close to the five-membered ring of the ligand (see the short distances reported in Figure 8c). Conversely, in the case of AMA, the  $\text{sp}^3$  ester carbon of the  $-\text{O}-\text{CH}_2-\text{CH}=\text{CH}_2$  moiety allows the chain to rotate away from the five-membered ring of the ligand, minimizing the unfavorable interaction between the  $-\text{OR}$  group of the growing chain and the metallocene skeleton (compare the value of 139° for the C2–O3–C4–C5 dihedral angle of AMA in Figure 8a with the value of  $-170^\circ$  for VMA in Figure 8c).

Moving to  $\text{C}_5$ -ligated catalyst **5**, with both monomers the favored TS involves the *si* face of the chain, which is located in an open part of the space away from the fluorenyl moiety of the

ligand (Figure 9a,c). Steric interaction between the monomer and the metallocene skeleton can be observed for both AMA and VMA. The competitive *re*-face TSs are disfavored by steric interaction between the chain and the ligand (see the short distances in Figure 9b,d). The rather similar  $\Delta G_{\text{Stereo}}$  values of 2.7 and 2.2 kcal/mol calculated for VMA and AMA, respectively, are in good agreement with the experimentally observed similar syndiotacticities of PVMA and PAMA (although the syndiotacticity of PVMA is somewhat higher than that of PAMA; vide supra).

**Postfunctionalization and Photo-Cross-Linking to Functional Materials.** Postfunctionalization of syndiotactic polymers bearing the pendant vinyl ( $-\text{CH}=\text{CH}_2$ ) functional group on every repeating unit was performed through two approaches: the thiol-ene “click” reaction and photocuring. The former approach has been widely used and proven to be highly effective for functionalization of ene-bearing polymers.<sup>29</sup> We first examined functionalization of *st*-PVMA ( $M_n = 40.9$  kg/mol,  $\bar{D} = 1.19$ ) and *st*-PDAA ( $M_n = 373$  kg/mol,  $\bar{D} = 1.43$ ) with two model thiols, 4-*tert*-butylbenzylmercaptan (RSH1) and 1-adamantanethiol (RSH2), using the click reaction with 2,2-dimethoxy-2-phenylacetophenone (DMPA) as the photoradical initiator under photochemical conditions (room temperature, UV lamp centered at  $\lambda = 350$  nm) in chloroform (Scheme 3).

**Scheme 3. Postfunctionalization of *st*-PVMA and *st*-PDAA via Thiol-ene “Click” Chemistry**



The pendant vinyl groups were completely converted into new  $-\text{CH}_2\text{CH}_2-\text{SR}$  groups, as confirmed by  $^1\text{H}$  NMR spectroscopy (Figures 10 and S5), which also showed that the tacticity of the resulting thiolated polymers was the same as that of the parent polymers in all cases. Gel-permeation chromatography analysis of the thiolated polymers, all of which are soluble in chloroform, showed an increase in the  $M_n$  and  $\bar{D}$  values (Figure S6), indicative of some degree of light cross-linking due to nonselective radical initiation in the presence of the high concentration of reactive  $\text{C}=\text{C}$  pendant groups. The thermal properties of the functionalized polymers were also significantly affected by the inclusion of the  $-\text{SR}$  groups. For instance, the first-step onset decomposition temperature ( $T_d$ ) of *st*-PVMA (234 °C) measured by thermogravimetric analysis (TGA) was enhanced by 62 °C to  $T_d = 296$  °C for both *st*-PVMA-SR1 and

*st*-PVMA-SR2 (Figure S7), attributed to the transformation of the  $-\text{OCH}=\text{CH}_2$  group into the  $-\text{OCH}_2\text{CH}_2\text{SR}$  moiety, which was accompanied by a change in  $T_g$  from 102 °C for *st*-PVMA to 39 and 118 °C for *st*-PVMA-SR1 and *st*-PVMA-SR2, respectively (Figure S8, top). In sharp contrast, *st*-PDAA exhibited a lower  $T_g$  (Figure S8, bottom) but higher thermal stability than its thiolated polymers *st*-PDAA-SR1 and *st*-PDAA-SR2 (Figure S9).

Because of the presence of the pendant vinyl groups, *st*-PVMA can also be readily photocured into flexible thin films for examination of their thermomechanical properties. Thus, a solvent-cast *st*-PVMA film was subjected to controlled cross-linking conditions under UV (350 nm) photoradical initiation with DMPA inside a Luzchem photoreactor for 10 min, producing a flexible, translucent, colorless thin film (*st*-PVMA-*h* $\nu$ ; Figure 11). A cross-linker, 1,4-benzenedimethanethiol (RSH3), was also added in varied amounts (2.5, 5, and 10 mol %) to prepare films with increased cross-linking and brittleness as the amount of RSH3 increases. Dynamic mechanical analysis (DMA) showed an increase in  $T_g$  going from the parent *st*-PVMA film (105 °C) to the photocured *st*-PVMA-*h* $\nu$  film (111 °C) after 10 min of UV irradiation, which was accompanied by increases in both storage modulus ( $E'$ ) and loss modulus ( $E''$ ) in both the glassy state (values reported at 25 °C) and the rubbery state (values reported at 150 °C) (Figure 12 and Table 2, entry 2 vs entry 1). Further increases in  $T_g$  (measured by the peak maxima of the  $\tan \delta$  ( $E''/E'$ ) curve in the DMA analysis) to 112, 121, and 128 °C were observed when the amount of the added cross-linker RSH3 was increased from 2.5 to 5.0 to 10 mol %, respectively (Table 2). This observed increasing  $T_g$  trend is a result of an increase in the degree of cross-linking, as characterized by the gradual increase in both  $E'$  and  $E''$  values in the rubbery state (values reported at 150 °C; Table 2, entries 3–5). On the other hand, the TGA traces for all of the thin films derived from *st*-PVMA were rather similar, displaying similar decomposition profiles (Figure S10). Likewise, a thin film of *st*-PDAA was also solvent-cast and subsequently photocured in the presence of 2 wt % DMPA. The resulting material, *st*-PDAA-*h* $\nu$ , exhibited a  $T_g$  of 56.1 °C as measured by DMA (Figure S11).

**Stereocomplexation and Photocuring To Form Robust Cross-Linked Stereocomplexes.** Stereocomplexes of diastereomeric polymer chains were formed effectively by mixing 10 mg/mL acetone solutions of *it*-PMMA and *st*-PVMA (designated *sc*-PMMA-PVMA; Figure 1) and of *it*-PMMA and *st*-PAMA (designated *sc*-PMMA-PAMA) at 40 °C in 1:1 and 1:2 *it*/*st* polymer ratios, which were left to slowly crystallize at room temperature to afford colorless, transparent thin films. The formation of such stereocomplexes was readily evident by the observation of a characteristic  $T_m$  peak in the DSC curves (Figures 13 and S12) and a characteristic diffraction peak at  $2\theta = 4.56^\circ$  ( $d = 1.94$  nm) in the pXRD patterns (Figure 14a).<sup>18</sup> Interestingly, the  $T_m$  of the stereocomplexes was not significantly affected by the molar ratio of the diastereomeric polymer pair tested (1:1 vs 1:2) but was sensitive to the molecular weight of the *it*-PMMA component (Table 3). For instance, *sc*-PMMA-PVMA showed  $T_m$  values of 165 and 164 °C (in 1:1 and 1:2 ratios, respectively) with *it*-PMMA having  $M_n = 26.4$  kg/mol ( $\bar{D} = 1.06$ ,  $[\text{mm}] = 92.2$ ), while the same stereocomplex displayed much higher  $T_m$  values of 188 and 186 °C (in 1:1 and 1:2 ratios, respectively) with *it*-PMMA having a much higher molecular weight ( $M_n = 136$  kg/mol,  $\bar{D} = 1.19$ ,  $[\text{mm}] = 96.4$ ). As expected, *it*-PAMA did not form a



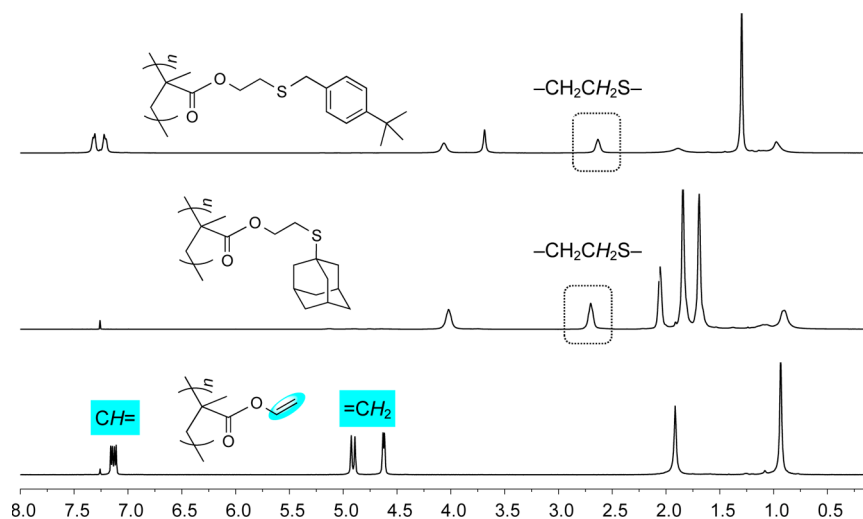


**Figure 10.** Overlay of  $^1\text{H}$  NMR spectra ( $\text{CDCl}_3$ ,  $25\text{ }^\circ\text{C}$ ) of *st*-PVMA (bottom), *st*-PVMA-SR1 (top), and *st*-PVMA-SR2 (middle).

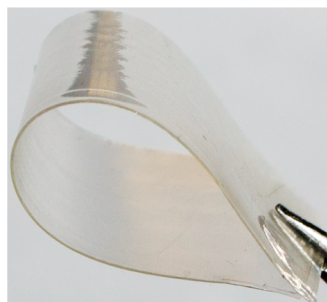


**Figure 11.** Photograph of a solvent-cast and photocured *st*-PVMA-*h* $\nu$  film (0.06 mm thick).

stereocomplex with either *st*-PAMA or *st*-PVMA in different ratios (1:1 and 1:2) and solvents (acetone and toluene), but

surprisingly, *it*-PAMA produced a weak stereocomplex with *st*-PMMA in both 1:1 and 1:2 ratios from their blends in acetone solutions, as revealed by broad transitions with  $T_m = 119\text{ }^\circ\text{C}$  (Figure 13a) and  $120\text{ }^\circ\text{C}$ , respectively. To further examine the effects of the ester group in the isotactic polymer chain on the formation of stereocomplexes, we also attempted the stereocomplexation between isotactic poly(*n*-butyl methacrylate) ( $[\text{mm}] = 96.9\%$ ,  $M_n \approx 28\text{ kg/mol}$ ) and *st*-PVMA or *st*-PAMA in acetone (complexing solvent) in 1:1 and 1:2 *it/st* molar ratios. However, the resulting materials showed only two  $T_g$  values corresponding to the constituent polymers, indicating that the stereocomplexation was hindered by the size of the *n*-butyl ester group of the isotactic polymer chain.

Control experiments in which *it*-PMMA was mixed with *st*-PVMA or *st*-PAMA in  $\text{CH}_2\text{Cl}_2$  in a 1:1 *it/st* ratio led to amorphous polymer blends that exhibited only the glass

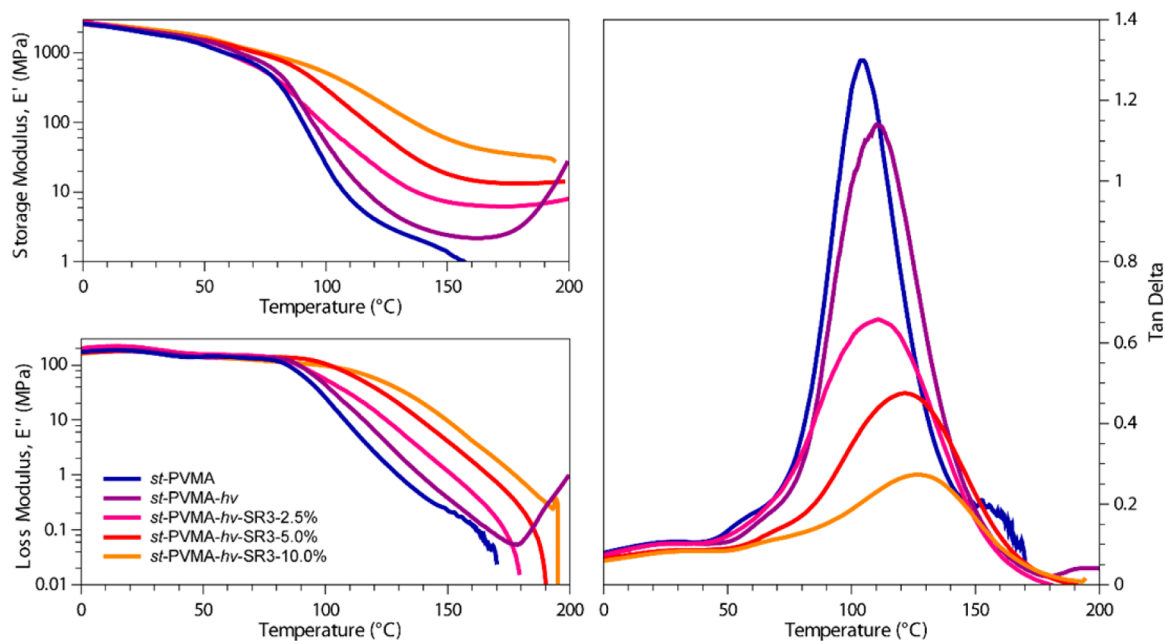


**Figure 12.** (top left) Storage modulus ( $E'$ ), (bottom left) loss modulus ( $E''$ ), and (right)  $\tan \delta$  ( $E''/E'$ ) of *st*-PVMA (blue), photocured *st*-PVMA-*h* $\nu$  (purple), *st*-PVMA-*h* $\nu$ -SR3-2.5% (pink), *st*-PVMA-*h* $\nu$ -SR3-5.0% (red), and *st*-PVMA-*h* $\nu$ -SR3-10.0% (orange) as determined by DMA analysis ( $3\text{ }^\circ\text{C min}^{-1}$  temperature ramp rate).

Table 2. Selected Thermomechanical Properties of Parent and Photocured Polymers As Characterized by DMA

entry	polymer	$T_g$ (°C)	$E'$ at 25 °C (GPa)	$E''$ at 25 °C (MPa)	$E'$ at 150 °C (MPa)	$E''$ at 150 °C (MPa)
1	<i>st</i> -PVMA	105	1.64	171	1.16	0.22
2	<i>st</i> -PVMA- <i>hν</i>	111	1.75	190	1.96	0.34
3	<i>st</i> -PVMA- <i>hν</i> -SR3-2.5%	112	1.73	178	6.00	0.95
4	<i>st</i> -PVMA- <i>hν</i> -SR3-5%	121	2.06	175	18.3	4.11
5	<i>st</i> -PVMA- <i>hν</i> -SR3-10%	128	1.32	107	34.5	5.67
6	<i>st</i> -PDAA- <i>hν</i>	56.1	1.04	90.7	49.8	5.47

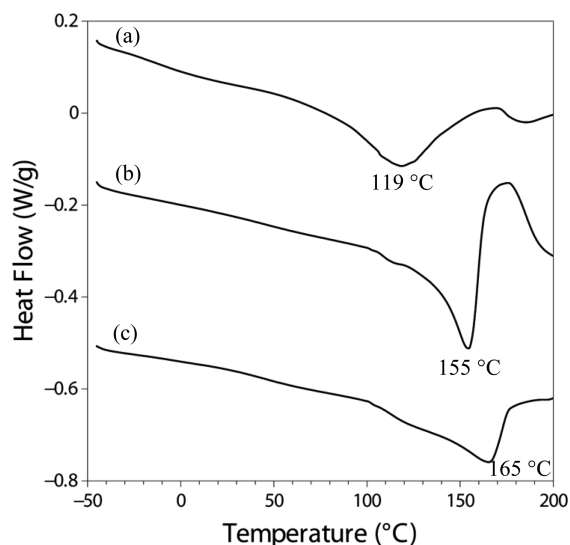


Figure 13. Representative DSC curves ( $10\text{ °C min}^{-1}$ ) for (a) *sc*-PAMA-PMMA (Table 3, entry 1), (b) *sc*-PMMA-PAMA (Table 3, entry 3), and (c) *sc*-PMMA-PVMA (Table 3, entry 11) obtained by crystallization from acetone solutions.

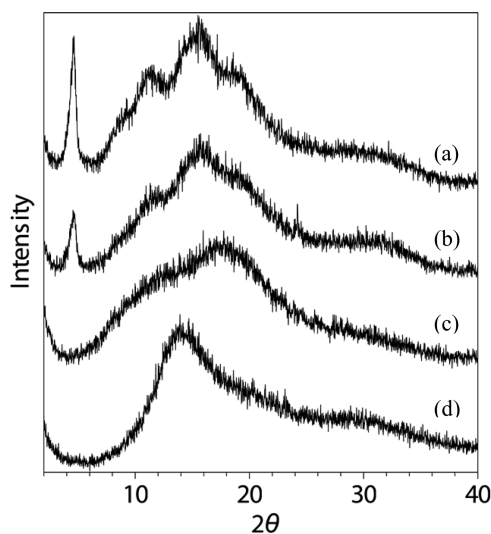


Figure 14. pXRD patterns of (a) *sc*-PMMA-PVMA and photo-cross-linked (b) *sc*-PMMA-PVMA-*hν*. The pXRD patterns of the constituent diastereomeric polymers (c) *st*-PVMA and (d) *it*-PMMA are included for comparison.

transitions corresponding to the constituent polymers of the blends, and typical cross-linking exotherms of the vinyl-containing polymers appeared at temperatures higher than  $150\text{ °C}$ . These results indicate that, just like *sc*-PMMA-PMMA,  $\text{CH}_2\text{Cl}_2$  is also a noncomplexing solvent for the stereocomplexes *sc*-PMMA-PVMA and *sc*-PMMA-PAMA, the for-

mation of which requires the use of a complexing solvent such as acetone or toluene.

Under UV ( $350\text{ nm}$ ) irradiation in the presence of the photoradical initiator DMPA, the stereocomplex *sc*-PMMA-PVMA was successfully photocured into the cross-linked, insoluble stereocomplex *sc*-PMMA-PVMA-*hν* (cf. Figure 1). The photocured stereocomplex exhibited a broad melting transition centered at  $\sim 150\text{ °C}$  (Figure S13) and a characteristic diffraction peak at  $2\theta = 4.56\text{ °C}$  ( $d = 1.94\text{ nm}$ ) (Figure 14b), thus confirming that the stereocomplex structure was retained after cross-linking. Thin films of *sc*-PMMA-PVMA and photo-cross-linked *sc*-PMMA-PVMA-*hν* were prepared and subsequently analyzed by DMA (Figure 15). While *it*-PMMA and *st*-PVMA showed single sharp glass transitions at  $T_g = 45.2$  and  $105\text{ °C}$ , respectively, as measured by the maxima of the  $\tan \delta$  curves, the stereocomplex sample *sc*-PMMA-PVMA showed two weak transitions at higher temperatures of  $62.2$  and  $135\text{ °C}$ . The photo-cross-linked samples *sc*-PMMA-PVMA-*hν* exhibited similar behavior with a shift of the transitions to even higher temperatures of  $67.2$  and  $158\text{ °C}$ , attributable to the cross-linking of the polymer networks. It is also noteworthy that the stereocomplex exhibited a considerably higher storage modulus than its constituents *it*-PMMA and *st*-PVMA at high temperatures and that the cross-linked stereocomplex had the highest modulus. For instance, at  $95\text{ °C}$ ,  $E'$  was measured to be  $0.713$ ,  $43.8$ ,  $175$ , and  $392\text{ MPa}$  for *it*-PMMA, *st*-PVMA, *sc*-PMMA-PVMA, and *sc*-PMMA-PVMA-*hν*, respectively. Overall, these thermomechanical and X-ray diffraction analysis results demonstrate that stereocomplex formation significantly increases the storage and loss moduli over those of the constituent *it* and *st* polymers at temperatures above  $100\text{ °C}$  and that the photocured stereocomplex retains the stereocomplex structure but with considerably enhanced thermal and mechanical properties of the material.

Besides the above-demonstrated enhanced thermal and mechanical properties of the cross-linked stereocomplexes, we anticipate another novel feature of the cross-linked stereocomplexes: they should be solvent-resistant and thus should not be decomplexed in a noncomplexing (or decomplexing) solvent such as chloroform, in contrast to the conventional *it*-PMMA/*st*-PMMA stereocomplex. To investigate this, we examined whether the *it*-PMMA helical chains can be trapped inside the stereocomplex cross-linked via the outer helical layer of the vinyl-containing *st* polymer. At the outset, a control experiment involving a sample of *sc*-PMMA (a mixture of *it*-PMMA and *st*-PMMA in 1:1 ratio) containing  $2\text{ wt } \%$  DMPA and subjected to UV irradiation ( $\lambda = 350\text{ nm}$ ) for  $2\text{ h}$  showed that the resulting stereocomplex was still completely soluble in chloroform and that no PMMA was trapped as a result of the absence of cross-linked chains. Using thermal cross-linking to trap the *it*-PMMA chains by annealing stereocomplex samples of *sc*-PMMA-PVMA and *sc*-PMMA-PAMA over  $200\text{ °C}$ , at which temperature thermal cross-linking occurs, was unsuccessful: while the

Table 3. Stereocomplexation and Photo-Cross-Linking Results<sup>a</sup>

entry	syndiotactic polymer	isotactic polymer	<i>st</i> / <i>it</i> molar ratio	$T_m^b$ (°C)	cross-linked vinyl polym. <sup>c</sup> (%)	trapped PMMA <sup>c</sup> (%)	PMMA trapping eff. <sup>c</sup> (%)
1	<i>st</i> -PMMA	<i>it</i> -PAMA	1:1	119	91.4	15.6	29
2	<i>st</i> -PAMA	—	—	—	97.2	—	—
3		low-MW <i>it</i> -PMMA	1:1	155	77.7	12.5	23.0
4		low-MW <i>it</i> -PMMA	2:1	157	85.8	20.0	29.9
5		high-MW <i>it</i> -PMMA	1:1	165	85.5	51.8	73.4
6		high-MW <i>it</i> -PMMA	2:1	168	84.7	50.5	67.2
7		( <i>it</i> -PMMA) <sub>0.83</sub> - <i>b</i> -( <i>it</i> -PAMA) <sub>0.17</sub>	1:1	168	63.7	49.1	86.7
8		( <i>it</i> -PMMA) <sub>0.67</sub> - <i>b</i> -( <i>at</i> -PVMA) <sub>0.33</sub>	1:1	170	79.0	63.0	89.6
9		( <i>it</i> -PMMA) <sub>0.88</sub> - <i>ran</i> -( <i>it</i> -PAMA) <sub>0.12</sub>	1:1	—	94.4	86.9	95.5
10	<i>st</i> -PVMA	—	—	—	58.3	—	—
11		low-MW <i>it</i> -PMMA	1:1	165	56.5	56.2	99.6
12		low-MW <i>it</i> -PMMA	2:1	164	56.2	13.5	31.4
13		high-MW <i>it</i> -PMMA	1:1	188	62.7	50.5	88.6
14		high-MW <i>it</i> -PMMA	2:1	186	54.1	39.0	78.7
15		( <i>it</i> -PMMA) <sub>0.83</sub> - <i>b</i> -( <i>it</i> -PAMA) <sub>0.17</sub>	1:1	181	66.4	58.5	93.9
16		( <i>it</i> -PMMA) <sub>0.67</sub> - <i>b</i> -( <i>at</i> -PVMA) <sub>0.33</sub>	1:1	182	71.1	59.8	92.6

<sup>a</sup>Polymer data: *st*-PAMA,  $M_n = 39.9$  kDa,  $\bar{D} = 1.45$ ,  $[rr] = 91.8$ ; *it*-PAMA,  $M_n = 32.4$  kDa,  $\bar{D} = 1.10$ ,  $[mm] = 96.5$ ; *st*-PVMA,  $M_n = 52.1$  kDa,  $\bar{D} = 1.31$ ,  $[rr] = 91.7$ ; *st*-PMMA,  $M_n = 36.3$  kDa,  $\bar{D} = 1.29$ ,  $[rr] = 93.7$ ; low-MW *it*-PMMA,  $M_n = 26.4$  kDa,  $\bar{D} = 1.06$ ,  $[mm] = 92.2$ ; high-MW *it*-PMMA,  $M_n = 136.1$  kDa,  $\bar{D} = 1.19$ ,  $[mm] = 96.4$ ; (*it*-PMMA)<sub>0.83</sub>-*b*-(*it*-PAMA)<sub>0.17</sub>,  $M_n = 89.6$  kDa,  $\bar{D} = 1.37$ ,  $[mm] = 93.1$ %; (*it*-PMMA)<sub>0.67</sub>-*b*-(*at*-PVMA)<sub>0.33</sub>,  $M_n = 76.8$  kDa,  $\bar{D} = 1.49$ ,  $[mm] = 79.8$ %, (*it*-PMMA)<sub>0.88</sub>-*ran*-(*at*-PAMA)<sub>0.12</sub>,  $M_n = 156$  kDa,  $\bar{D} = 1.83$ ,  $[mm] = 95.9$ %. <sup>b</sup> $T_m$  measured by DSC. <sup>c</sup>See the SI for the quantification method.

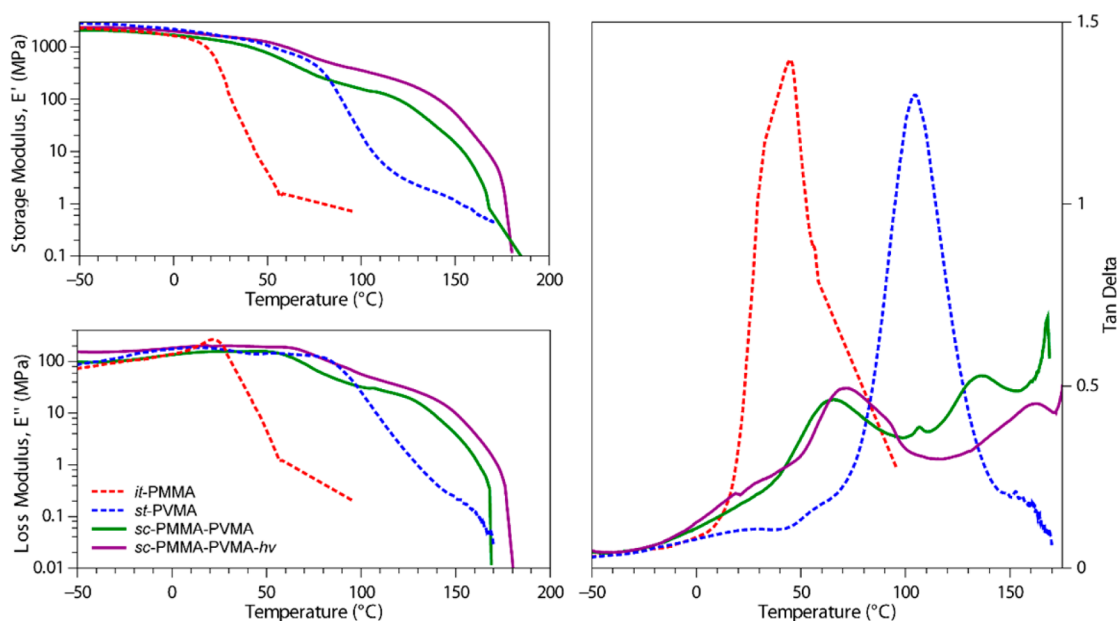
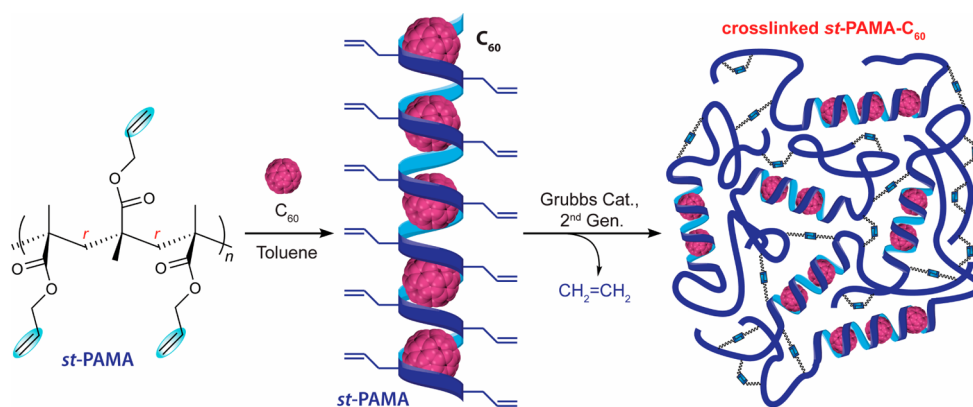


Figure 15. (top left) Storage modulus ( $E'$ ), (bottom left) loss modulus ( $E''$ ), and (right)  $\tan \delta$  ( $E''/E'$ ) of *it*-PMMA (red), *st*-PVMA (blue), *sc*-PMMA-PVMA (green), and *sc*-PMMA-PVMA- $h\nu$  (purple) as determined by DMA analysis ( $3^\circ\text{C min}^{-1}$  temperature ramp rate).

*st* polymer was successfully cross-linked at this temperature, the *it*-PMMA chains were released from the melt. Next, *sc*-PMMA-PVMA and *sc*-PMMA-PAMA were photo-cross-linked with 2 wt % DMPA under UV irradiation ( $\lambda = 350$  nm) for 2 h at room temperature. The cross-linked material was extracted with chloroform (a decomplexing solvent) for 24 h at  $40^\circ\text{C}$  to promote the possible release of the complexed but untrapped *it*-PMMA. The amount of cross-linked *st* polymer as well as the trapped *it*-PMMA was quantified by  $^1\text{H}$  NMR analysis (see the SI). The *it*-PMMA trapping efficiency was calculated as the percentage of the experimental *it*-PMMA content (wt %) found versus the theoretical *it*-PMMA content in the cross-linked stereocomplex if all of the initial *it*-PMMA were effectively

trapped. Table 3 summarizes our study of the *it*-PMMA trapping efficiency as a function of (a) the *it*-PMMA molecular weight, (b) the molar ratio of *it*-PMMA to *st*-PVMA (or *st*-PAMA), and (c) use of block and random copolymers incorporating the photo-cross-linkable units.

The results summarized in Table 3 show that a control sample of *st*-PAMA afforded a much higher degree of cross-linking (97.2%) compared with *st*-PVMA (58.3%) when they were photocured under the same conditions. Similarly, stereocomplexes containing both *it*-PAMA and *st*-PAMA samples were more effectively photo-cross-linked (from 63.7% to 91.4% degree of cross-linking) than those containing *st*-PVMA (which achieved only 54.1% to 71.1%). It should be



**Figure 16.** Schematic representation of the formation of the *ic*-PAMA- $C_{60}$  inclusion complex and its cross-linking via olefin metathesis.

**Table 4. Results of Complexation between *st*-PAMA and  $C_{60}$  and Subsequent Cross-Linking by Olefin Metathesis<sup>a</sup>**

entry	<i>st</i> -PAMA concentration (mg mL <sup>-1</sup> )	$C_{60}$ concentration (mg mL <sup>-1</sup> )	solvent	$T_g^b$ (°C)	$T_m^b$ (°C)	yield after cross-linking (%) <sup>c</sup>	encapsulated $C_{60}$ content (wt %) <sup>d</sup>
1	5.0	1.0	Tol	47.9	200	n.d.	n.d.
2	5.0	2.0	Tol	53.1	206	n.d.	n.d.
3	10.0	1.0	Tol	53.6	207	>99	3.39
4	10.0	2.0	Tol	52.8	205	>99	4.77
5	10.0	10.0	Tol-DCB	56.3	207	>99	9.18
6	20.0	1.0	Tol	52.6	—	n.d.	n.d.
7	20.0	2.0	Tol	55.1	211	n.d.	n.d.
8	20.0	10.0	Tol-DCB	57.3	207	n.d.	n.d.

<sup>a</sup>Conditions: 2.0 mL of solvent (Tol = toluene or Tol-DCB = 1:1 (v/v) toluene/1,2-dichlorobenzene), except for entries 1 and 2 (5.0 mL); Grubbs second-generation catalyst (2 mol %); *st*-PAMA ( $M_n$  = 39.9 kDa,  $\bar{D}$  = 1.45,  $[rr]$  = 91.8); n.d. = not determined. <sup>b</sup> $T_g$  and  $T_m$  before cross-linking measured by DSC. <sup>c</sup>Determined by gravimetric measurements. <sup>d</sup>Calculated by TGA.

noted that the self-cross-linking ability of *st*-PVMA in a sample crystallized from a  $CH_2Cl_2$  solution (Table S1) was higher (82.4%), indicating that the crystallization conditions impact the self-cross-linking ability of *st*-PVMA in the solid state. Under both conditions tested (acetone and  $CH_2Cl_2$ ), *st*-PAMA showed considerably better self-cross-linking ability (>95%) compared with *st*-PVMA, indicating that the longer, more flexible allyl ester group can be more efficiently cross-linked than the shorter, more rigid vinyl group in the VMA repeat unit. Stereocomplexes of *sc*-PMMA-PAMA with high-MW *it*-PMMA ( $M_n$  = 136.1 kg/mol,  $\bar{D}$  = 1.19) achieved a higher PMMA trapping efficiency (up to 73.4%; entry 5) than those stereocomplexes with low-MW *it*-PMMA ( $M_n$  = 26.4 kg/mol,  $\bar{D}$  = 1.06) (up to 29.9%; entry 4). No correlation was observed between the PMMA trapping efficiency and the molar ratio of the diastereomeric polymer pair. To possibly further enhance the PMMA trapping efficiency, we employed a new strategy of using block copolymers of *it*-PMMA with PAMA and PVMA to form stereocomplexes with *st*-PAMA and *st*-PVMA. Indeed, the PMMA trapping efficiency was enhanced to 86.7 and 89.6% (entries 7 and 8), indicating that a portion of the cross-linkable block is also photocured. The highest PMMA trapping efficiency of 95.5% (entry 9) was obtained from a blend of *st*-PAMA with a random copolymer, (*it*-PMMA)<sub>0.88</sub>-*ran*-(*it*-PAMA)<sub>0.12</sub>, but the stereocomplexation was hindered by the random placement of AMA units in the *it*-PMMA chain. In comparison, the PMMA trapping efficiency was generally higher (up to quantitative) for the stereocomplexes formed with *st*-PVMA (entries 11–16) than for those with *st*-PAMA (entries 3–9). Again, higher PMMA trapping efficiencies were observed when block copolymers containing cross-linkable

AMA or VMA units were employed as the isotactic component to form the stereocomplex (>92.6%; entries 15 and 16).

Additional control studies used non-stereocomplexed control samples prepared by mixing *it*-PMMA with *st*-PVMA or *st*-PAMA in a noncomplexing solvent ( $CH_2Cl_2$ ) and photocuring under conditions identical to those reported for Table 3. The samples were further analyzed to quantify the capacity of the cross-linked *st*-vinyl polymers to trap *it*-PMMA, and the results are summarized in Table S1. The *it*-PMMA trapping efficiency was almost negligible (0.6 to 2.6%), indicating that the photocross-linked polymer blends are not capable of trapping the *it*-PMMA chains. These control experiments highlight the importance of the polymer supramolecular structure for efficient trapping of the *it*-PMMA chains, which is achievable only when the stereocomplexes are formed. For instance, while the *sc*-PMMA-PVMA formed in acetone had a PMMA trapping efficiency of 99.6% (Table 3, entry 11), the same mixture made in  $CH_2Cl_2$  showed a PMMA trapping efficiency of only 2.6% (Table S1, entry 4).

We also investigated the possible complexation of *st*-PVMA and *st*-PAMA with fullerene  $C_{60}$  to form an inclusion complex, *ic*-PVMA- $C_{60}$  or *ic*-PAMA- $C_{60}$ . The material formed by *st*-PVMA and  $C_{60}$  exhibited a broad melting transition peak at temperature >150 °C, which was overlapped with many intense exothermic peaks (due to thermally induced cross-linking), thus offering no clear evidence for the formation of the inclusion complex. However, we obtained conclusive evidence that *st*-PAMA readily forms inclusion complexes, *ic*-PAMA- $C_{60}$  (Figure 16), with  $C_{60}$  in different ratio combinations (Table 4). The formation of such inclusion complexes was evidenced by the appearance of a sharp melting transition from 200 to 211

°C (Figure 17) observed by DSC analysis of the resulting product after crystallization. The DSC thermograms of

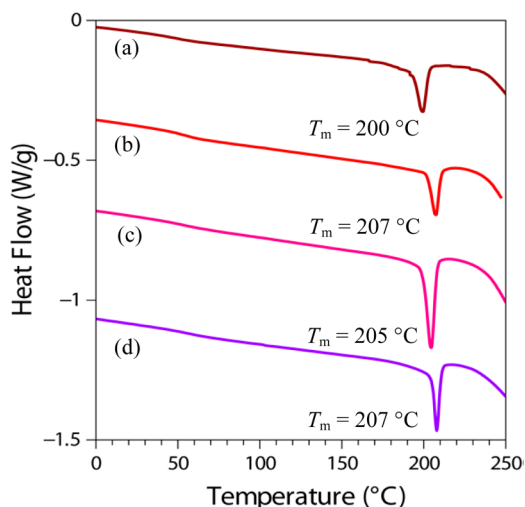


**Figure 17.** DSC thermograms ( $10\text{ }^{\circ}\text{C min}^{-1}$ ) of *ic*-PAMA- $\text{C}_{60}$  produced from toluene solutions of *st*-PAMA and  $\text{C}_{60}$ : Table 4, entry 1 (a), entry 3 (b), entry 4 (c), and entry 8 (d).

commercial fullerene  $\text{C}_{60}$ , *st*-PAMA, a non-inclusion-complex mixture of *st*-PAMA and  $\text{C}_{60}$  (obtained by annealing of the blend at  $80\text{ }^{\circ}\text{C}$  for 20 h), and *ic*-PAMA- $\text{C}_{60}$  are shown in Figure 18 for comparison. The first-order transition in the DSC

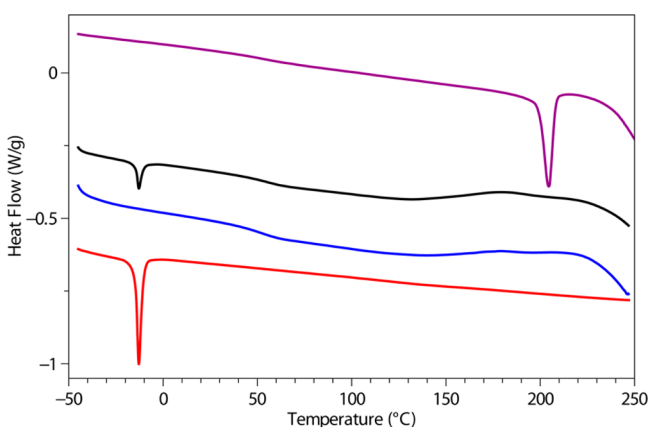


**Figure 18.** DSC thermograms ( $10\text{ }^{\circ}\text{C min}^{-1}$ ) of commercial fullerene  $\text{C}_{60}$  powder (red), *st*-PAMA (blue), *st*-PAMA/ $\text{C}_{60}$  blend annealed at  $80\text{ }^{\circ}\text{C}$  for 20 h (black), and *ic*-PAMA- $\text{C}_{60}$  from Table 4, entry 4 (purple).

thermogram of  $\text{C}_{60}$  corresponds to the well-known phase transition between a simple cubic (sc) lattice (below  $T_{\text{tr}} = -14.8\text{ }^{\circ}\text{C}$ ) and a face-centered cubic (fcc) lattice.<sup>30</sup> *st*-PAMA shows a  $T_{\text{g}}$  of  $49.9\text{ }^{\circ}\text{C}$  plus a broad thermal cross-linking exothermic peak at temperature  $>150\text{ }^{\circ}\text{C}$ , whereas the non-inclusion-complex mixture of *st*-PAMA and  $\text{C}_{60}$  shows both mentioned features of the individual components. In sharp contrast, the *ic*-PAMA- $\text{C}_{60}$  complex obtained by crystallization from toluene exhibits a novel feature: a markedly sharp melting transition at  $T_{\text{m}} = 205\text{ }^{\circ}\text{C}$ , indicative of the formation of the inclusion complex.

Three approaches were explored to produce cross-linked *ic*-PAMA- $\text{C}_{60}$ . First, photochemically induced radical cross-linking

with DMPA as the initiator under UV irradiation ( $\lambda = 350\text{ nm}$ ) in solution or the solid state did not produce the cross-linked product, as the crystallized material was again completely soluble in toluene. Second, thermally induced radical cross-linking with benzoyl peroxide (BPO) as the initiator also failed to afford the target cross-linked *ic*-PAMA- $\text{C}_{60}$ . Third, recognizing  $\text{C}_{60}$  as an excellent radical trap,<sup>31</sup> we turned our attention to nonradical cross-linking methods. To this end, successful cross-linking of *ic*-PAMA- $\text{C}_{60}$  was achieved using 2 mol % second-generation Grubbs catalyst<sup>32</sup> in toluene at room temperature for 2 h (Figure 16 and Table 4, entries 3–5). However, the DSC thermogram of the material obtained from the solution-phase metathesis cross-linking of *ic*-PAMA- $\text{C}_{60}$  exhibited no melting transition peak but a  $T_{\text{g}}$  of  $106\text{ }^{\circ}\text{C}$ , which is about  $50\text{ }^{\circ}\text{C}$  higher than that of the parent *st*-PAMA. This result indicates that most, if not all, of the helical inclusion complex structure was disrupted by this solution cross-linking reaction to form a mostly amorphous cross-linked structure (Figure 16).

After successful cross-linking, the  $\text{C}_{60}$  encapsulated inside the network of cross-linked *st*-PAMA- $\text{C}_{60}$  could not be reversibly recovered by dissolution of the inclusion complex because it was no longer soluble in toluene. A control reaction was performed to assess the amount of Ru catalyst residue in the cross-linked complex by performing a cross-linking reaction of *st*-PAMA under the same conditions but without  $\text{C}_{60}$ . The content of  $\text{C}_{60}$  in the cross-linked complex was calculated through TGA analysis (Figure 19) by subtracting the residue in

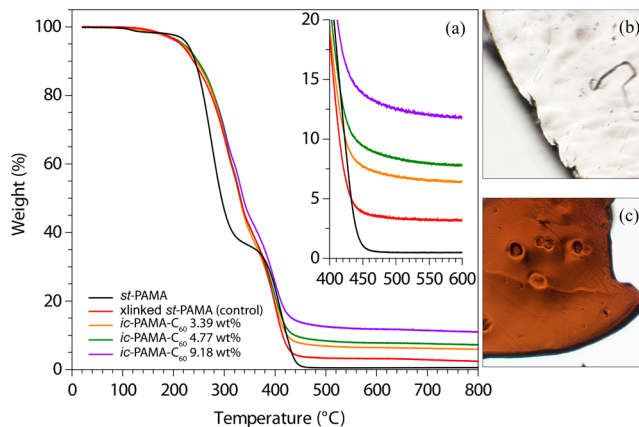


**Figure 19.** (a) TGA traces ( $10\text{ }^{\circ}\text{C min}^{-1}$ ) of *st*-PAMA (black), cross-linked *st*-PAMA control (red), cross-linked *ic*-PAMA- $\text{C}_{60}$  3.43 wt % (orange), cross-linked *ic*-PAMA- $\text{C}_{60}$  4.77 wt % (green), and cross-linked *ic*-PAMA- $\text{C}_{60}$  9.18 wt % (purple). (b) Microphotograph of an *st*-PAMA film sample. (c) Microphotograph of the cross-linked *ic*-PAMA- $\text{C}_{60}$  4.77 wt % film.

the trace at  $500\text{ }^{\circ}\text{C}$  for *st*-PAMA- $\text{C}_{60}$  minus that in the control experiment (3.49 wt %). These results indicated a  $\text{C}_{60}$  uptake of up to 9.18 wt % in the cross-linked *st*-PAMA- $\text{C}_{60}$  when a  $10.0\text{ mg/mL}$  solution of  $\text{C}_{60}$  in the feed was employed.

## CONCLUSIONS

The perfectly chemoselective and highly syndiospecific coordination polymerization of divinyl polar monomers developed through this work has enabled the synthesis of highly syndiotactic polar vinyl polymers bearing a pendant reactive  $\text{C}=\text{C}$  bond on each repeat unit. Polymerizations of three representative polar divinyl monomers (AMA, VMA, and

DAA) by the  $C_s$ -ligated zirconocenium ester enolate catalysts under ambient conditions all achieved complete chemoselectivity and high stereoselectivity, producing the corresponding vinyl-functionalized polymers with syndiotacticities following this trend: *st*-PDAA (>99% *rr*) > *st*-PVMA (96% *rr*) > *st*-PAMA (92% *rr*). Careful examination of the polymerization of VMA by catalyst **5**, including synthetic, kinetic, and mechanistic studies, showed that the polymerization follows a unimetallic, enantiomeric-site-controlled mechanism through a cationic cyclic metallacycle resting intermediate and exhibits the ability to control the resulting polymer  $M_n$  and  $D$  values. DFT calculations of the free energies  $\Delta G_{\text{Stereo}}$  of the transition state geometries for the competitive (correct and incorrect enantiofacial) additions in the polymerizations of AMA and VMA provided a theoretical basis for the observed large difference in isotacticity of the polymers produced by  $C_2$ -ligated catalyst **1** but the rather similar syndiotacticities of the polymers produced by  $C_3$ -ligated catalyst **5**.

The pendant vinyl groups of the obtained syndiotactic polymers can be completely converted into the corresponding thiolated polymers of the same tacticity via thiol-ene click reactions with different thiols. Such polymers can also be readily photocured into flexible, cross-linked thin films for examination of their thermomechanical properties, which revealed an expected increase in  $T_g$ ,  $E'$ , and  $E''$  values as the degree of cross-linking increases.

The vinyl-functionalized syndiotactic polymers *st*-PVMA and *st*-PAMA can readily form crystalline stereocomplexes with *it*-PMMA in a 2:1 or 1:1 molar ratio, but *st*-PVMA appears to form a stronger stereocomplex, as evidenced by the observed higher  $T_m$ , presumably because of the higher syndiotacticity of the constituent *st*-PVMA. Interestingly, *it*-PAMA also forms a weak stereocomplex with *st*-PMMA, and the isotactic block copolymers *it*-PMMA-*b*-*it*-PAMA and *it*-PMMA-*b*-*st*-PVMA, but not their random copolymers, readily form crystalline stereocomplexes with either *st*-PAMA or *st*-PVMA; both findings extended the *it* polymers capable of stereocomplexation beyond *it*-PMMA. The *it* /*st* stereocomplex *sc*-PMMA-PVMA can be readily photocured into a cross-linked, insoluble stereocomplex that exhibits high *it*-PMMA trapping efficiencies. Thermomechanical and X-ray diffraction analyses showed that stereocomplex formation significantly increases the storage and loss moduli over those of the constituent *it* and *st* polymers at temperatures above 100 °C and that the photocured stereocomplex retains the stereocomplex structure but with considerably enhanced thermal and mechanical properties of the material.

*st*-PAMA readily forms inclusion complexes, *ic*-PAMA- $C_{60}$ , with  $C_{60}$  in different ratio combinations. Cross-linking of *ic*-PAMA- $C_{60}$  was achieved successfully via olefin metathesis using the Grubbs second-generation catalyst, whereas photocuring in the presence of a photoinitiator was unsuccessful because  $C_{60}$  is an excellent radical trap. The encapsulated  $C_{60}$  in the resulting cross-linked *st*-PAMA- $C_{60}$  cannot be released by dissolution of the inclusion complex, in contrast to the un-cross-linked inclusion complex.

## ■ ASSOCIATED CONTENT

### ● Supporting Information

The Supporting Information is available free of charge on the ACS Publications website at DOI: 10.1021/jacs.6b04064.

Full experimental details, additional figures and tables, and computational details (PDF)

## ■ AUTHOR INFORMATION

### Corresponding Authors

\*luigi.cavallo@kaust.edu.sa

\*eugene.chen@colostate.edu

### Notes

The authors declare no competing financial interest.

## ■ ACKNOWLEDGMENTS

This work was supported by the U.S. National Science Foundation (NSF-1300267) for the study carried out at Colorado State University. L. Cavallo thanks the HPC team of Enea ([www.enea.it](http://www.enea.it)) for use of the ENEA-GRID and the HPC facilities CRESCO ([www.cresco.enea.it](http://www.cresco.enea.it)) in Portici, Italy. We thank Boulder Scientific Co. for the research gifts of  $B(C_6F_5)_3$  and  $[Ph_3C][B(C_6F_5)_4]$ .

## ■ REFERENCES

- (1) Selected reviews: (a) *Stereoselective Polymerization with Single-Site Catalysts*; Baugh, L. S., Canich, J. A. M., Eds.; CRC Press: Boca Raton, FL, 2008. (b) Resconi, L.; Chadwick, J. C.; Cavallo, L. In *Comprehensive Organometallic Chemistry III*; Bochmann, M., Vol. Ed.; Mingos, D. M. P., Crabtree, R. H.; Series Eds.; Elsevier: Oxford, U.K., 2007; Vol. 4, pp 1005–1166. (c) Coates, G. W. *Chem. Rev.* **2000**, *100*, 1223–1252. (d) Brintzinger, H. H.; Fischer, D.; Mülhaupt, R.; Rieger, B.; Waymouth, R. M. *Angew. Chem., Int. Ed. Engl.* **1995**, *34*, 1143–1170.
- (2) Selected recent examples and reviews: (a) Jian, Z.; Baier, M. C.; Mecking, S. *J. Am. Chem. Soc.* **2015**, *137*, 2836–2839. (b) Ota, Y.; Ito, S.; Kuroda, J.; Okumura, Y.; Nozaki, K. *J. Am. Chem. Soc.* **2014**, *136*, 11898–11901. (c) Nakamura, A.; Anselment, T. M. J.; Claverie, J. P.; Goodall, B.; Jordan, R. F.; Mecking, S.; Rieger, B.; Sen, A.; van Leeuwen, P. W. N. M.; Nozaki, K. *Acc. Chem. Res.* **2013**, *46*, 1438–1449. (d) Delferro, M.; Marks, T. J. *Chem. Rev.* **2011**, *111*, 2450–2485. (e) Nakamura, A.; Ito, S.; Nozaki, K. *Chem. Rev.* **2009**, *109*, 5215–5244. (f) Berkefeld, A.; Mecking, S. *Angew. Chem., Int. Ed.* **2008**, *47*, 2538–2542. (g) Luo, S.; Vela, J.; Lief, G. R.; Jordan, R. F. *J. Am. Chem. Soc.* **2007**, *129*, 8946–8947. (h) Domski, G. J.; Rose, J. M.; Coates, G. W.; Bolig, A. D.; Brookhart, M. *Prog. Polym. Sci.* **2007**, *32*, 30–92. (i) Jensen, T. R.; Yoon, S. C.; Dash, A. K.; Luo, L.; Marks, T. J. *J. Am. Chem. Soc.* **2003**, *125*, 14482–14494. (j) Gibson, V. C.; Spitzmesser, S. K. *Chem. Rev.* **2003**, *103*, 283–315. (k) Coates, G. W.; Hustad, P. D.; Reinartz, S. *Angew. Chem., Int. Ed.* **2002**, *41*, 2236–2257. (l) Ittel, S. D.; Johnson, L. K.; Brookhart, M. *Chem. Rev.* **2000**, *100*, 1169–1204.
- (3) Selected reviews: (a) Soller, B. S.; Salzinger, S.; Rieger, B. *Chem. Rev.* **2016**, *116*, 1993–2022. (b) Chen, E. Y.-X. *Chem. Rev.* **2009**, *109*, 5157–5214. (c) Yasuda, H. *Prog. Polym. Sci.* **2000**, *25*, 573–626.
- (4) Selected examples: (a) Zhang, N.; Salzinger, S.; Soller, B. S.; Rieger, B. *J. Am. Chem. Soc.* **2013**, *135*, 8810–8813. (b) Chen, X.; Caporaso, L.; Cavallo, L.; Chen, E. Y.-X. *J. Am. Chem. Soc.* **2012**, *134*, 7278–7281. (c) Miyake, G. M.; Mariott, W. R.; Chen, E. Y.-X. *J. Am. Chem. Soc.* **2007**, *129*, 6724–6725. (d) Lian, B.; Spaniol, T. P.; Okuda, J. *Organometallics* **2007**, *26*, 6653–6660. (e) Lian, B.; Thomas, C. M.; Navarro, C.; Carpentier, J.-F. *Organometallics* **2007**, *26*, 187–195. (f) Stojcevic, G.; Kim, H.; Taylor, N. J.; Marder, T. B.; Collins, S. *Angew. Chem., Int. Ed.* **2004**, *43*, 5523–5526. (g) Strauch, J. W.; Fauré, J.-L.; Bredeau, S.; Wang, C.; Kehr, G.; Fröhlich, R.; Luftmann, H.; Erker, G. *J. Am. Chem. Soc.* **2004**, *126*, 2089–2104. (h) Frauenrath, H.; Keul, H.; Höcker, H. *Macromolecules* **2001**, *34*, 14–19. (i) Bandermann, F.; Ferenz, M.; Sustmann, R.; Sicking, W. *Macromol. Symp.* **2001**, *174*, 247–253. (j) Cameron, P. A.; Gibson, V.; Graham, A. J. *Macromolecules* **2000**, *33*, 4329–4335. (k) Li, Y.; Ward, D. G.; Reddy, S. S.; Collins, S. *Macromolecules* **1997**, *30*, 1875–1883. (l) Deng, H.; Shiono, T.; Soga, K. *Macromolecules* **1995**, *28*, 3067–3073.

- (m) Collins, S.; Ward, S. G. *J. Am. Chem. Soc.* **1992**, *114*, 5460–5462.
- (n) Yasuda, H.; Yamamoto, H.; Yokota, K.; Miyake, S.; Nakamura, A. *J. Am. Chem. Soc.* **1992**, *114*, 4908–4909.
- (5) (a) Gao, H.; Matyjaszewski, K. *Prog. Polym. Sci.* **2009**, *34*, 317–350. (b) Li, Z.; Day, M.; Ding, J.; Faid, K. *Macromolecules* **2005**, *38*, 2620–2625. (c) Percec, V.; Auman, B. C. *Makromol. Chem.* **1984**, *185*, 2319–2336.
- (6) Selected examples: (a) Sugiyama, F.; Satoh, K.; Kamigaito, M. *Macromolecules* **2008**, *41*, 3042–3048. (b) Ma, J.; Cheng, C.; Sun, G. R.; Wooley, K. L. *Macromolecules* **2008**, *41*, 9080–9089. (c) Vardareli, T. K.; Keskin, S.; Usanmaz, A. *J. Macromol. Sci., Part A: Pure Appl. Chem.* **2008**, *45*, 302–311. (d) Paris, R.; de la Fuente, J. L. *J. Polym. Sci., Part A: Polym. Chem.* **2005**, *43*, 6247–6261. (e) Paris, R.; de la Fuente, J. L. *J. Polym. Sci., Part A: Polym. Chem.* **2005**, *43*, 2395–2406. (f) Nagelsdiek, R.; Mennicken, M.; Maier, B.; Keul, H.; Höcker, H. *Macromolecules* **2004**, *37*, 8923–8932.
- (7) Pugh, C.; Percec, V. *Polym. Bull.* **1985**, *14*, 109–116.
- (8) Selected examples: (a) Mohan, Y. M.; Raghunadh, V.; Sivaram, S.; Baskaran, D. *Macromolecules* **2012**, *45*, 3387–3393. (b) Lu, Z.; Lee, S. Y.; Goh, S. H. *Polymer* **1997**, *38*, 5893–5895. (c) Fukuda, W.; Nakao, M.; Okumura, K.; Kakiuchi, H. *J. Polym. Sci., Part A-1: Polym. Chem.* **1972**, *10*, 237–250.
- (9) Chen, E. Y.-X. *Top. Curr. Chem.* **2012**, *334*, 239–260.
- (10) (a) Chen, J.; Chen, E. Y.-X. *Isr. J. Chem.* **2015**, *55*, 216–225. (b) Jia, Y.-B.; Ren, W.-M.; Liu, S.-J.; Xu, T.; Wang, Y.-B.; Lu, X.-B. *ACS Macro Lett.* **2014**, *3*, 896–899.
- (11) Xu, T.; Liu, J.; Lu, X.-B. *Macromolecules* **2015**, *48*, 7428–7434.
- (12) Bolig, A. D.; Chen, E. Y.-X. *J. Am. Chem. Soc.* **2004**, *126*, 4897–4906.
- (13) Rodriguez-Delgado, A.; Chen, E. Y.-X. *Macromolecules* **2005**, *38*, 2587–2594.
- (14) (a) Mariott, W. R.; Chen, E. Y.-X. *Macromolecules* **2005**, *38*, 6822–6832. (b) Mariott, W. R.; Chen, E. Y.-X. *Macromolecules* **2004**, *37*, 4741–4743.
- (15) Vidal, F.; Gowda, R. R.; Chen, E. Y.-X. *J. Am. Chem. Soc.* **2015**, *137*, 9469–9480.
- (16) Selected examples of *sc*-PMMA: (a) Ren, J. M.; Satoh, K.; Goh, T. K.; Blencowe, A.; Nagai, K.; Ishitake, K.; Christofferson, A. J.; Yiapanis, G.; Yarovsky, I.; Kamigaito, M.; Qiao, G. G. *Angew. Chem., Int. Ed.* **2014**, *53*, 459–464. (b) Goh, T. K.; Tan, J. F.; Guntari, S. N.; Satoh, K.; Blencowe, A.; Kamigaito, M.; Qiao, G. G. *Angew. Chem., Int. Ed.* **2009**, *48*, 8707–8711. (c) Kawauchi, T.; Kumaki, J.; Yashima, E. *J. Am. Chem. Soc.* **2006**, *128*, 10560–10567. (d) Kawauchi, T.; Kumaki, J.; Okoshi, K.; Yashima, E. *Macromolecules* **2005**, *38*, 9155–9160. (e) Serizawa, T.; Hamada, K.-I.; Akashi, M. *Nature* **2004**, *429*, 52–55. (f) Slager, J.; Domb, A. J. *Adv. Drug Delivery Rev.* **2003**, *55*, 549–583. (g) Serizawa, T.; Hamada, K.; Kitayama, T.; Fujimoto, N.; Hatada, K.; Akashi, M. *J. Am. Chem. Soc.* **2000**, *122*, 1891–1899. (h) Hatada, K.; Kitayama, T.; Ute, K.; Nishiura, T. *Macromol. Symp.* **1998**, *132*, 221–230. (i) te Nijenhuis, K. *Adv. Polym. Sci.* **1997**, *130*, 67–81. (j) Spevacek, J.; Schneider, B. *Adv. Colloid Interface Sci.* **1987**, *27*, 81–150. (k) Watanabe, W. H.; Ryan, C. F.; Fleischer, P. C., Jr.; Garrett, B. S. *J. Phys. Chem.* **1961**, *65*, 896–896. (l) Fox, T. G.; Garrett, B. S.; Goode, W. E.; Gratch, S.; Kincaid, J. F.; Spell, A.; Stroupe, J. D. *J. Am. Chem. Soc.* **1958**, *80*, 1768–1769.
- (17) (a) Christofferson, A. J.; Yiapanis, G.; Ren, J. M.; Qiao, G. G.; Satoh, K.; Kamigaito, M.; Yarovsky, I. *Chem. Sci.* **2015**, *6*, 1370–1378. (b) Kumaki, J.; Kawauchi, T.; Ute, K.; Kitayama, T.; Yashima, E. *J. Am. Chem. Soc.* **2008**, *130*, 6373–6380. (c) Kumaki, J.; Kawauchi, T.; Okoshi, K.; Kusanagi, H.; Yashima, E. *Angew. Chem., Int. Ed.* **2007**, *46*, 5348–5351. (d) Schomaker, E.; Challa, G. *Macromolecules* **1989**, *22*, 3337–3341. (e) Bosscher, G.; ten Brinke, G.; Eshuis, A.; Challa, G. *Macromolecules* **1982**, *15*, 1364–1368. (f) Kusanagi, H.; Tadokoro, H.; Chatani, Y. *Macromolecules* **1976**, *9*, 531–532. (g) Liquori, A. M.; Anzuino, G.; Coiro, V. M.; D'Alagni, M.; de Santis, P.; Savino, M. *Nature* **1965**, *206*, 358–362.
- (18) (a) Asai, S.; Kawano, T.; Hirota, S.-I.; Tominaga, Y.; Sumita, M.; Mizumoto, T. *Polymer* **2007**, *48*, 5116–5124. (b) Schomaker, E.; Challa, G. *Macromolecules* **1988**, *21*, 2195–2203. (c) Bosscher, F.; ten Brinke, G.; Challa, G. *Macromolecules* **1982**, *15*, 1442–1444.
- (19) (a) Hatada, K.; Kitayama, T.; Ute, K.; Fujimoto, N.; Miyatake, N. *Macromol. Symp.* **1994**, *84*, 113–126. (b) Kitayama, T.; Fujimoto, N.; Hatada, K. *Polym. Bull.* **1991**, *26*, 629–636.
- (20) Escudé, N. C.; Ning, Y.; Chen, E. Y.-X. *Polym. Chem.* **2012**, *3*, 3247–3255.
- (21) Mariott, W. R.; Escudé, N. C.; Chen, E. Y.-X. *J. Polym. Sci., Part A: Polym. Chem.* **2007**, *45*, 2581–2592.
- (22) Mariott, W. R.; Chen, E. Y.-X. *J. Am. Chem. Soc.* **2003**, *125*, 15726–15727.
- (23) Escudé, N. C.; Chen, E. Y.-X. *Chem. Mater.* **2009**, *21*, 5743–5753.
- (24) (a) Kusuyama, H.; Miyamoto, N.; Chatani, Y.; Tadokoro, H. *Polym. Commun.* **1983**, *24*, 119–122. (b) Kusuyama, H.; Takase, M.; Higashihata, Y.; Tseng, H.-T.; Chatani, Y.; Tadokoro, H. *Polymer* **1982**, *23*, 1256–1258.
- (25) (a) Kawauchi, T.; Kitaura, A.; Kawauchi, M.; Takeichi, T.; Kumaki, J.; Iida, H.; Yashima, E. *J. Am. Chem. Soc.* **2010**, *132*, 12191–12193. (b) Kawauchi, M.; Kawauchi, T.; Takeichi, T. *Macromolecules* **2009**, *42*, 6136–6140. (c) Kawauchi, T.; Kitaura, A.; Kumaki, J.; Kusanagi, H.; Yashima, E. *J. Am. Chem. Soc.* **2008**, *130*, 11889–11891. (d) Kawauchi, T.; Kumaki, J.; Kitaura, A.; Okoshi, K.; Kusanagi, H.; Kobayashi, K.; Sugai, T.; Shinohara, H.; Yashima, E. *Angew. Chem., Int. Ed.* **2008**, *47*, 515–519.
- (26) (a) Zhang, Y.; Ning, Y.; Caporaso, L.; Cavallo, L.; Chen, E. Y.-X. *J. Am. Chem. Soc.* **2010**, *132*, 2695–2709. (b) Ning, Y.; Chen, E. Y.-X. *J. Am. Chem. Soc.* **2008**, *130*, 2463–2465.
- (27) Zhang, Y.; Caporaso, L.; Cavallo, L.; Chen, E. Y.-X. *J. Am. Chem. Soc.* **2011**, *133*, 1572–1588.
- (28) (a) Caporaso, L.; Cavallo, L. *Macromolecules* **2008**, *41*, 3439–3445. (b) Caporaso, L.; Gracia-Budria, J.; Cavallo, L. *J. Am. Chem. Soc.* **2006**, *128*, 16649–16654.
- (29) Selected reviews: (a) Barner-Kowollik, C.; Du Prez, F. E.; Espeel, P.; Hawker, C. J.; Junkers, T.; Schlaad, H.; Van Camp, W. *Angew. Chem., Int. Ed.* **2011**, *50*, 60–62. (b) Hoyle, C. E.; Bowman, C. N. *Angew. Chem., Int. Ed.* **2010**, *49*, 1540–1573. (c) Iha, R. K.; Wooley, K. L.; Nyström, A. M.; Burke, D. J.; Kade, M. J.; Hawker, C. J. *Chem. Rev.* **2009**, *109*, 5620–5686. (d) Binder, W. H.; Sachsenhofer, R. *Macromol. Rapid Commun.* **2008**, *29*, 952–981. (e) Binder, W. H.; Sachsenhofer, R. *Macromol. Rapid Commun.* **2007**, *28*, 15–54.
- (30) (a) Skokan, E. V.; Alioshina, V. E.; Spiridonov, F. M.; Arkhangelsky, I. V.; Davydov, V. Y.; Tamm, N. B.; Sidorov, L. N. *J. Phys. Chem.* **1995**, *99*, 16116–16118. (b) Saito, R.; Dresselhaus, G.; Dresselhaus, M. S. *Phys. Rev. B: Condens. Matter Mater. Phys.* **1994**, *49*, 2143–2147. (c) Fischer, J. E.; Luzzi, D. E.; Kniáz, K.; McGhie, A. R.; Ricketts-Foot, D. A.; Romanow, W. R.; Vaughan, G. B. M.; Heiney, P. A.; Li, D.; Smith, A. L.; Strongin, R. M.; Cichy, M. A.; Brard, L.; Smith, A. B. *Phys. Rev. B: Condens. Matter Mater. Phys.* **1993**, *47*, 14614–14617. (d) Heiney, P. A.; Fischer, J. E.; McGhie, A. R.; Romanow, W. J.; Denenstein, A. M.; McCauley, J. P., Jr.; Smith, A. B.; Cox, D. E. *Phys. Rev. Lett.* **1991**, *66*, 2911–2914.
- (31) Tzirakis, M. D.; Orfanopoulos, M. *Chem. Rev.* **2013**, *113*, 5262–5321.
- (32) Scholl, M.; Ding, S.; Lee, C. W.; Grubbs, R. H. *Org. Lett.* **1999**, *1*, 953–956.